



# Experimental and predictive modelling in dry micro-drilling of titanium alloy using Ti–Al–N coated carbide tools

P. Prashanth<sup>1</sup> · Somashekhar S. Hiremath<sup>1</sup>

Received: 17 March 2022 / Accepted: 23 August 2022 / Published online: 13 September 2022  
© The Author(s), under exclusive licence to Springer-Verlag France SAS, part of Springer Nature 2022

## Abstract

In a rapidly changing manufacturing environment, accurate and efficient models are necessary to predict cutting force and feature quality in the mechanical micro-drilling process. Micro-drilling is challenging due to high spindle speeds and size effects and, therefore, cannot be considered a scaled-down version of macro-drilling. In this study, micro-holes of  $\varnothing$  0.4 mm are machined using Ti–Al–N coated carbide micro-drill on Titanium alloy (Cp-Ti grade 2) under dry conditions. The process parameters like cutting speed, feed, and pecking depth are varied in three levels based on the full-factorial design with thrust force, burr height, and radial overcut as responses. Predictive models are developed for responses using two intelligent modelling techniques: generalised regression neural network (GRNN) and adaptive neuro-fuzzy inference system (ANFIS). The experimental data is used to train models, and additional experiments are performed to generate testing and validation data. Later multiple regression analysis (MRA) models are also developed for responses. The results indicated that the predicted responses from GRNN, ANFIS, and MRA errors are within  $\pm 5\%$ ,  $\pm 5.5\%$ , and  $\pm 12\%$ , respectively, suggesting that the GRNN and ANFIS models are more reliable than the MRA model. In this research, the GRNN models outperformed the ANFIS models. In continuation of the study, optimal process parameters are ascertained to minimize responses simultaneously. At optimal parameter settings, the performance of uncoated and Ti–Al–N coated carbide micro-drills is also evaluated by experiments. Ti–Al–N coated micro-drill reduces the considered responses with lesser tool wear and a favourable chip formation compared to the uncoated micro-drill.

**Keywords** Dry micro-drilling · Ti–Al–N coated micro-drill · GRNN modelling ANFIS modelling multi-response optimization

## Abbreviations

MMD	Mechanical micro drilling
PCB	Printed circuit board
MQL	Minimum quantity lubrication
ANN	Artificial neural network
ANFIS	Artificial neuro-fuzzy inference system
GRNN	Generalized regression neural network
MRA	Multiple regression analysis
RSM	Response surface methodology
AI	Artificial intelligence
MF	Membership function
FIS	Fuzzy inference systems
CV	Coefficient of variation

MAPE Maximum absolute prediction error

## 1 Introduction

Titanium alloy (Cp-Ti grade 2) is used extensively in the biomedical industry for fabricating medical implants, filters, and micro-catheters due to bio-compatibility [1]. In these applications, machining of micro-holes of desired quality is essential [2, 3].

Micro-holes are machined using both conventional and non-conventional micromachining processes. The non-conventional processes include electro-discharge machining, electrochemical machining, abrasive jet machining, laser beam machining, and electron beam machining. Among conventional micro-machining processes, micro-holes are machined using a rotating micro-drill on a stationary workpiece by direct contact in Mechanical Micro Drilling

✉ Somashekhar S. Hiremath  
somashekhar@iitm.ac.in

<sup>1</sup> Department of Mechanical Engineering, Indian Institute of Technology Madras, Chennai, Tamilnadu 600036, India

(MMD) process. MMD process is preferred over other non-conventional processes because the better quality holes can be machined in less time [4].

Dry micro-drilling is gaining much importance in many biomedical applications, as there is a requirement for cleaner production [5], and cutting fluids can cause contamination. The biomedical implants make direct contact with the human tissues during their usage [6], and contamination has to be minimized to avoid infections [7].

However executing MMD under dry conditions on Titanium alloy (Cp-Ti grade 2) poses significant challenges as it is a difficult to machine material because of low thermal conductivity, affinity with cutting tools, and strain hardening behaviour. Due to low thermal conductivity high temperatures are generated at chip-tool interface resulting in an accelerated tool wear [8]. Moreover micro-drills used in MMD are slender with a higher flute length to diameter ratio and susceptible to breakages [9]. Therefore, selecting a suitable drilling strategy, process parameters, and tools becomes vital.

Continuous and peck drilling strategies are mainly used for machining in MMD. The temperature at the chip-tool interface decreases with the peck drilling strategy as holes are machined with intermittent feed-in steps [10]. In MMD, peck drilling is observed better than continuous drilling in improving hole dimensional accuracy and roundness due to better chip clearance [11]. Peck drilling is also found effective in improving tool life when machining micro-holes of smaller aspect ratios [12, 13]. Even though the machining time is higher in peck drilling than continuous drilling; it improves tool life by avoiding frequent drill breakages and minimizes tooling costs.

For increasing tool life, selection of pecking depth is critical. In literature, 10% of the drill diameter is suggested for MMD of stainless steel [14], whereas in another study on nickel-based super alloy was varied from 0.05 to 0.5 mm with  $\varnothing$  0.5 mm drill [15]. Therefore pecking depth selection mainly depends on the combination of tool, work-piece, and machining condition.

The coated micro-drills are used effectively in the dry machining of various engineering materials. The effect of chromium-based multi-layered coatings on tungsten carbide micro-drills was investigated in MMD of Printed Circuit Board (PCB), Cr-Si -Al-N coating with 8.7% silicon content effectively reduced tool wear and improved hole quality [16]. Similarly, another study on MMD of PCB investigated the effect of nitrogen percentages in Zirconium chromium nitride-based coatings on tungsten carbide micro drills. Coating with 17% nitrogen effectively improved tool life and hole quality [17]. Among the various coated tools, the Ti-Al-N coated micro-drills are used successfully in MMD of hard-cut materials. Imran et al. [18] investigated the tool wear

mechanism in MMD of Inconel 718. They optimized the cutting conditions for increasing tool life using Ti-Al-N coated micro-drills under wet conditions. The tool wear mechanism was analysed, and significant causes were identified as abrasion, microchipping, and adhesion. In another study, Ti-Al-N coated micro-drills were also found effective in the reduction of entry burr height in MMD of Nickel-based super-alloy Nimonic 80A [19].

Many studies in the past were carried out on MMD of titanium alloys on the tool, process parameter selection and optimization of responses. Giorleo et al. [20] evaluated the performance of  $Al_2O_3$  coated HSS micro-drill of  $\varnothing$  0.5 mm in MMD of Titanium grade 2 material using direct drilling strategy under dry conditions with tool life and hole roundness as measured responses. The  $Al_2O_3$  coating effectively enhanced the tool life, whereas it had a negligible effect on hole roundness error.

Guu et al. [21] studied effect of process parameters spindle speed (5000, 12,000, 20,000) rpm, feed (1, 2, 3) mm/min, and tool holder length (10, 15, 20) on responses stress concentration and hole quality in MMD of Ti-6Al-4 V. Experiments were conducted under wet conditions with three different coolants with an uncoated Tungsten carbide micro-drill of  $\varnothing$  0.2 mm using a direct drilling strategy. A finite element analysis model was developed to determine stress concentration. An increase in stress concentration influenced the hole quality adversely.

Prasanna et al. [22] optimized process parameters such as spindle speed (2000, 3500, 5000) rpm, feed rate (5, 10, 15) mm/min, under air blow condition by varying air pressure (2, 4, 6) bars for output responses like thrust force, radial overcut, circularity, and taper angle in MMD of Ti-6Al-4 V. Air blow condition was selected for experimentation using  $\varnothing$  0.4 mm uncoated carbide micro-drill adopting direct drilling strategy. Thrust force was influenced mainly by spindle speed and feed, whereas spindle speed and air pressure significantly impacted hole quality.

The effect of different cooling conditions like dry, wet, Minimum Quantity Lubrication (MQL), and cryogenic cooling on responses like thrust force, torque, exit burr height, tool wear, and surface roughness in MMD of Ti-6Al-4 V with tungsten carbide micro-drill of  $\varnothing$  0.7 mm [23]. Experiments were performed by direct drilling strategy with varying process parameters spindle speed: (1000, 25,000, 5000, and 7500) rpm and feed rates (5, 10, 15, 30, 50) mm/min. Among various cooling conditions, cryogenic was influential in reducing both tool wear and exit burr height. Similarly, the effect of nano-diamond particle-based Minimum Quantity Lubrication (MQL) on responses thrust force, torque, tool wear, and circularity in MMD of Ti-6Al-4 V were investigated [24]. The experiments were carried out using uncoated tungsten carbide micro-drills of  $\varnothing$  0.3 mm by direct drilling strategy. Nano-particle size and concentration were

optimized for responses, and a significant reduction in all the responses was observed with particle size of 35 nano-meters, 0.4% weight concentration and feed rate of 10 mm/min. Mechanistic models for responses like exit burr height and thrust force were developed in MMD of Ti–6Al–4 V [25]. The experiments were carried out by direct drilling in wet conditions using an uncoated tungsten carbide micro-drill of  $\varnothing 0.3$  mm. Experimental results were in good agreement with the results predicted by the model.

Even though much information is available on the MMD of titanium alloys, whenever there is a change in tool type, workpiece material, drilling strategy, and machining conditions, the process parameters must be selected optimally to enhance hole quality and minimize thrust forces. In regular practice, the operator has to perform numerous experiments to identify the optimal parameters. This trial and error approach extends the time needed for preparation before processing and results in resource wastages. Therefore to avoid the drawbacks of the trial and error approach, it becomes necessary to develop appropriate models for predicting output responses quickly and accurately when there is a change in process parameters [26].

Regression analysis is a statistical modelling technique that establishes the relationship between input variables and output responses. It is ideally suited to develop models to predict output responses when many independent variables are present. However, the major disadvantage of adopting statistical modelling techniques is their greater dependence on model-structural assumptions, whether linear or nonlinear, which results in uncertainty in the model's prediction performance [27]. Therefore Artificial Intelligence (AI) based techniques like Adaptive Neural Networks (ANN) and Fuzzy Logic (FL) are adopted for developing predictive models to overcome these disadvantages.

ANN are mathematical simulations of the biological nervous system that mimic its behaviour. They have distributed, simultaneous, and adaptive computing that can map complicated, nonlinear systems, which are difficult to map using regression methods [28]. An ANN is a potent mathematical tool that has demonstrated its effectiveness in various domains [29]. The sample size has a significant impact on the traditional ANN. Usually, a large number of samples are needed to ensure the accuracy of the prediction. Many variants of ANN like GRNN and ANFIS are developed to overcome these limitations.

GRNN is a probabilistic neural network developed by Specht in 1991, mainly applied for regression and function approximation. GRNN is advantageous compared to traditional ANN as only a smaller proportion of the training data is necessary. Because a probabilistic neural network can connect to the underlying function of the data even when using a limited number of training samples [27]. GRNN is based on a one-pass training algorithm; therefore, it speeds up the

training process and trains the network more quickly. Unlike traditional feed-forward networks, GRNN estimation can always converge to a global solution [30]. The GRNN is also found very effective in modelling many non-conventional machining process [27, 31].

ANFIS is a hybrid technique that combines the fuzzy behaviour of a fuzzy inference system with the high-learning capabilities of an ANN developed by Jang [32]. The ANN can self-understand the data patterns, and fuzzy logic applies if–then rules to manage existing uncertainty and imprecision. Since it combines both neural networks and fuzzy logic principles, it can capture both benefits in a single frame. In the ANFIS technique, a fuzzy model is developed initially based on rules extracted from the system's input and output data. The ANN is later utilized to fine-tune the fuzzy rules to obtain the ANFIS model. ANFIS models are also used successfully in other fields of mechanical engineering due to its advantages [32–34]

In past studies on MMD, statistical and Artificial Intelligence (AI) based methods are used to develop predictive models for responses as presented in Table 1.

Past studies on predictive modelling in the MMD process reveal that uncoated carbide micro-drill is used. Using a Ti–Al–N coated carbide micro-drill in the MMD process, researchers have not attempted to develop predictive models for thrust force and quality features like burr height and radial overcut. Even though several AI models have been tried in the MMD process, the GRNN modelling technique has not been attempted in spite of its advantages. There are very few research studies that compare the performance of AI-based models and regression models in conventional micro-machining processes.

Therefore, the current study aims to develop GRNN, ANFIS, and MRA models for thrust force, burr height, and radial overcut in MMD of Titanium alloy (Cp-Ti grade 2) using Ti–Al–N coated carbide micro-drills under dry conditions, with cutting speed, feed, and pecking depth as process parameters.

The study has been extended to determine process parameter settings in order to simultaneously minimize responses by multi-response optimization. The experiments are also carried out using an uncoated carbide micro-drill at optimal settings, and the results are compared with Ti–Al–N coated carbide drill.

## 2 Materials and methods

In the current study, Titanium alloy (CP-Ti grade 2) is selected as workpiece material, its chemical composition is tested using optical emission spectroscopy and presented in Table 2.

**Table 1** Statistical and AI based predictive modelling in MMD process

Sl. No	Author/year	Work piece material/machining condition	Tool/drilling strategy	Process parameters/experimental design	Responses	Modeling method
1	Shanmugam et al. (2011)[4]	Glass fiber reinforced polymer Dry	Solid carbide micro-drill (Ø 0.32 mm) Direct, peck drilling	Spindle speed, feed Full factorial	Thrust force, torque	Non-linear power models
2	Patra et al. (2015) [35]	Austenitic stainless steel Dry	Uncoated carbide micro-drill (Ø 0.5 mm) Direct drilling	Cutting speed and feed Full factorial	Thrust force, lateral forces,	Response surface methodology (RSM)
3	Ahn et al. (2016) [36]	Brass and copper Dry	Tungsten carbide micro drill (Ø 0.3 mm and Ø 0.5 mm) Direct drilling	Cutting speed, feed, drill diameter, hardness ratio and tensile strength Full factorial	Burr type	Artificial Neural Network (ANN)
4	K patra et al. (2017) [37]	Tool steel (AISI P20) Air cooling	High speed steel micro-drill Ø 0.5 mm Peck drilling	Cutting speed, feed, thrust force, number of holes machined Full factorial	Tool wear	ANN
5	Anand et al. (2018) [38]	Carbon fiber reinforced polymer Dry	Uncoated carbide micro-drill (Ø 0.5 mm) Direct drilling	Cutting speed and feed Full factorial	Thrust force, radial forces, roundness error, de-lamination factor	RSM
6	Huang et al. (2020) [39]	Aluminum 7075-T6 alloy Nano fluid minimum quantity lubrication	Tungsten carbide micro drill Ø 0.2 mm Peck drilling	Cutting speed, feed, and pecking depth, Nano diamond weight, Distance of Nozzle, MQL Flow, Angle of Nozzle and air Compression Taguchi L18	Thrust force, Torque	ANN
7	Ranjan et al. (2020) [40]	Austenitic stainless steel SS316 Dry	Tungsten carbide micro drill Ø 0.4 mm Peck drilling	Thrust force, torque and vibration signals Five conditions with different cutting speed and feed	Hole roundness error	ANFIS

**Table 2** Chemical composition of Titanium alloy—(Cp-Ti grade 2)

Sl No	Element	Composition (%)
1	Titanium	99.70
2	Carbon	0.031
3	Chromium	0.02
4	Nitrogen	0.02
5	Oxygen	0.010
6	Ferrous	0.13

**Table 3** Tool specification

Sl No	Parameter	Specification
1	Total length	38.0 mm
2	Drill diameter	Ø 0.4 mm
3	Flute length	6.0 mm
4	Shank diameter	Ø 3.157 mm
5	Helix angle	30°
6	Point angle	130°
7	Drill material	Tungsten carbide
8	Coating type	Ti–Al–N

Workpieces of size 40 × 20 × 1 mm are prepared for experimentation.

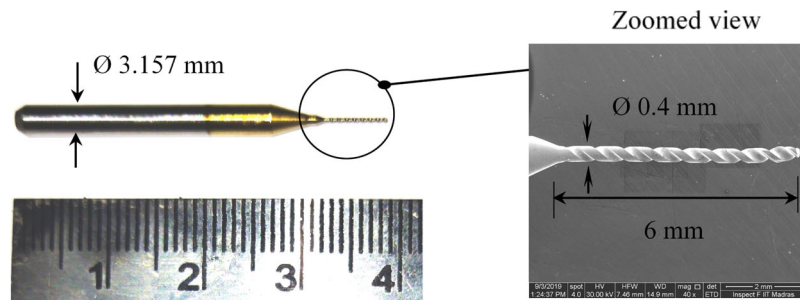
Commercially available Ti–Al–N coated carbide micro-drills of Ø 0.4 mm are used for experiments, and the specification is shown in Table 3. Figure 1a depicts the image of the micro-drill used in the study. The coating on micro-drill is confirmed using Energy Dispersive Spectroscopy (EDS), and results are depicted in Fig. 1b.

### 2.1 Experimental design and setup

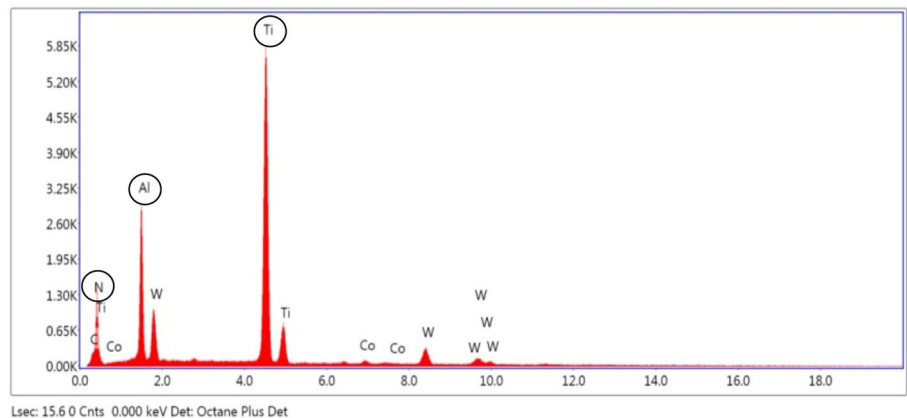
A full factorial design presented in Table 4 by varying process parameters like cutting speed, feed, and pecking depth in three levels is adopted for experimentation. The levels of process parameters are selected based on preliminary experimentation and the literature survey.

Experiments are carried out on a 3-axis vertical machining centre (KMI118 of JYOTI make) and the specification of machine is presented in Table 5. The work-pieces are secured firmly on vice and mounted on a multi-component dynamometer of Kistler make (9257B). Finally, the dynamometer is connected to a charge amplifier type 5070 of Kistler make and data acquisition system compatible with *dynoware* software. The schematic of the experimental setup is presented in Fig. 2.

**Fig. 1** Details of Ti–Al–N coated micro-drill used for experimentation



**(a)** Micro –drill image



**(b)** EDS graph



**Table 4** Experimental design

SI No	Parameter	Symbol	Levels		
			- 1	0	+ 1
1	Cutting speed (m/min)	V	8.8	13.8	18.8
2	Feed ( $\mu\text{m}/\text{rev}$ )	F	4	8	12
3	Pecking depth ( $\mu\text{m}$ )	P	25	50	75

**Table 5** Specification of machine used for experimentation

SI No	Parameter	Specification
1	Maximum spindle speed	15,000 rpm
2	Spindle power	15 kW
3	Spindle torque	110/84 Nm
4	Positioning accuracy	10 $\mu\text{m}$
5	Positioning repeatability	5 $\mu\text{m}$
6	Table length	800 mm
7	Table width	600 mm

## 2.2 Measurement procedure for responses

The thrust force, exit burr height, and radial overcut are the three responses measured in this study, and the procedure for measuring them is discussed in this section.

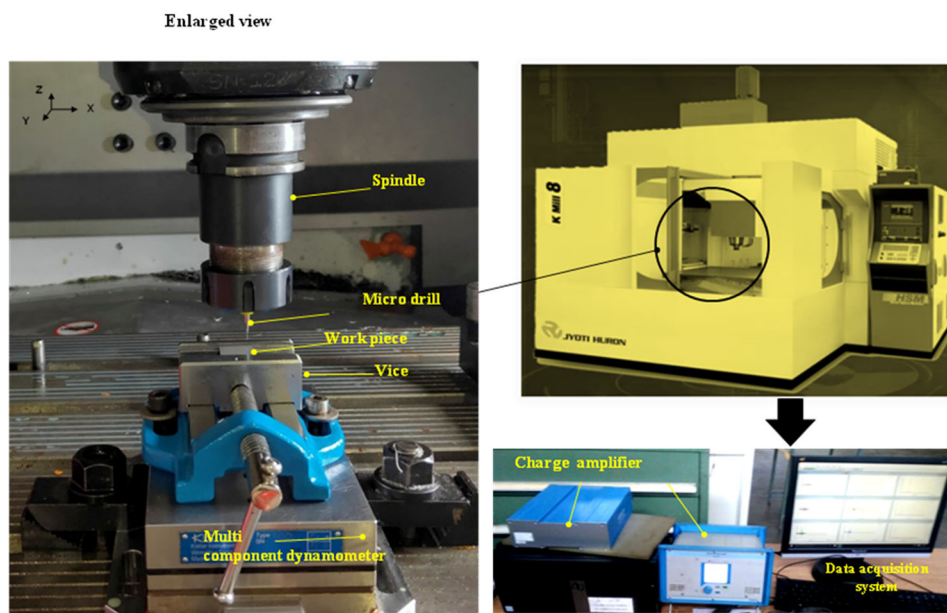
### 2.2.1 Thrust force

Thrust forces are relatively higher when machined with micro-drills than the larger diameter drills due to longer

chisel edge length compared with its diameter [41]. Moreover, the micro-drills are slender with larger flute length to diameter, and larger thrust forces can reduce tool life due to breakages. Therefore it is necessary to minimize thrust forces for increasing tool life.

The thrust force signals are captured at a 1500 Hz/s sampling rate using a multi-component dynamometer. The signals are further amplified using a charge amplifier and transferred to a data acquisition system, and a low pass filter is applied to eliminate noise.

The maximum value of thrust force is considered for each hole [4]. A typical recorded thrust force signal is presented in Fig. 3, and three distinct stages can be identified [42]. In stage 1, a gradual increase in thrust force is observed as the micro-drill contacts the work-piece during entry. As the drill penetrates, thrust force becomes steady, as observed in stage 2. A decrease in thrust force can be observed in stage 3, as the drill exits the work-piece material. Therefore the maximum value is considered for each hole from the thrust force signal for analysis.

**Fig. 2** Experimental setup

**Fig. 3** Thrust force variation at  $V = 18.8$  m/min,  $F = 4$   $\mu$ m/rev and  $P = 75$   $\mu$ m

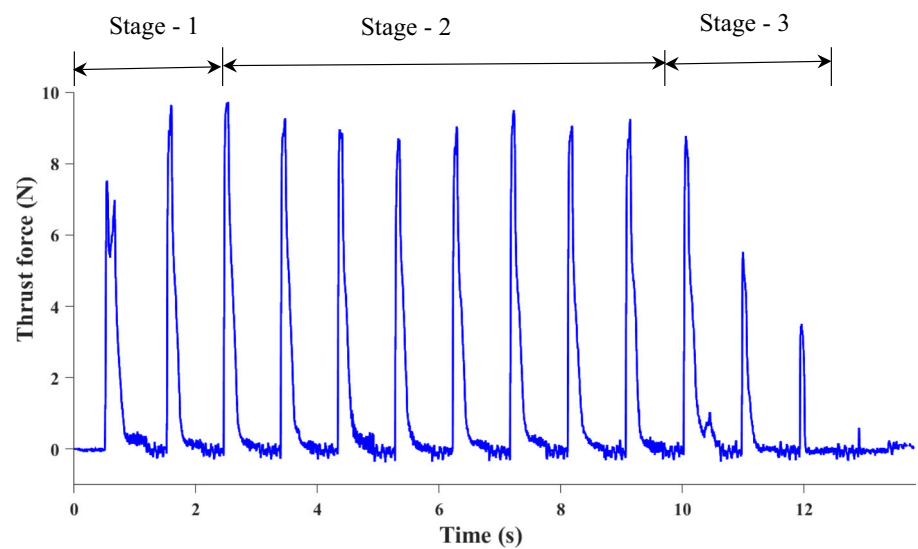
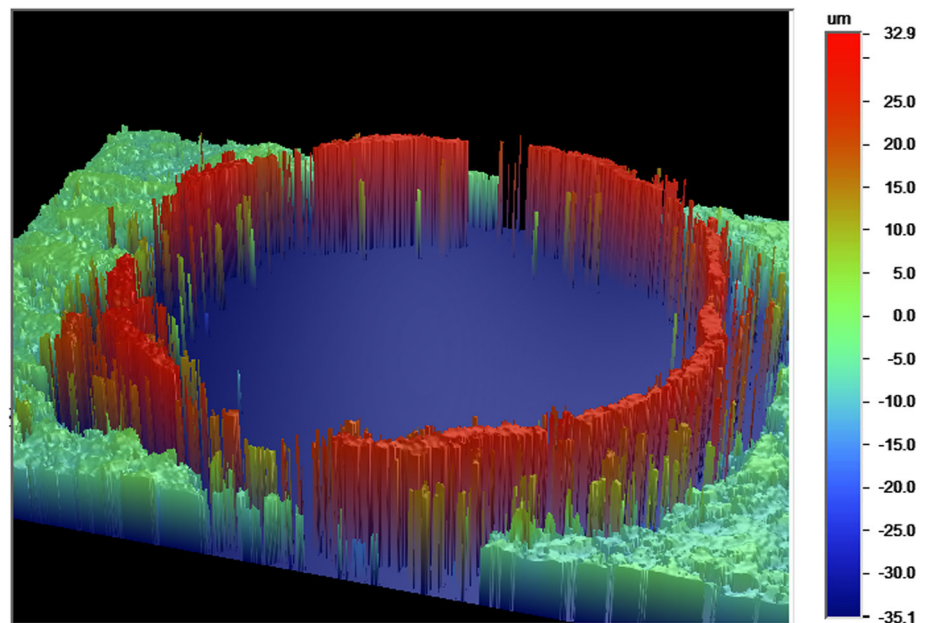


**Fig. 4** 3D profiler burr height measurement



### 2.2.2 Burr height

Burrs are undesirable material projections generated on both micro-drill entry and exit surfaces of work-piece. In the drilling of titanium alloys, the exit burrs are larger and more challenging to remove than entry burr. Therefore exit burr formation is of significant interest in the current study, as burr elimination or reduction minimizes manufacturing time and costs.

The burr formation is mainly characterized by burr height and burr thickness; among them, burr thickness remains stable and does not vary much with process parameters [43] compared to burr height. Therefore burr height is characterized and measured using a non-contact 3D profiler of VEECO

make. The hole is scanned, and maximum burr height is considered [44] as indicated on the digital scale for analysis, Fig. 4 shows a typical burr height measurement.

### 2.2.3 Radial overcut

The machined holes are characterized for dimensional accuracy by measuring radial overcut. The diameter of machined holes on the entry side is larger than the exit side due to wandering motion [21, 24] and therefore considered for analysis. The images of machined holes are captured using a stereomicroscope, and diameter is measured by selecting 8 points on the hole periphery using image processing software *Image-j* [45]. The radial overcut is determined using Eq. 1, based on the measured hole diameter on entry side  $D_{entry}$  and the tool

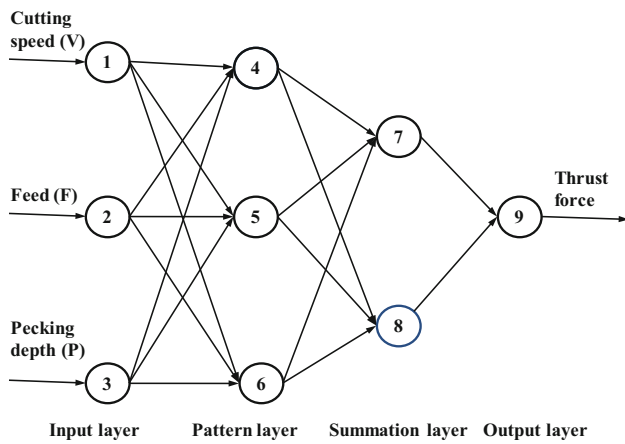


Fig. 5 Block diagram of GRNN architecture

$D_{tool}$  [46]

$$Radial\ overcut(\mu m) = \left( \frac{D_{entry} - D_{tool}}{2} \right) \tag{1}$$

### 2.3 Generalised regression neural network (GRNN)

GRNN model mainly consists of four different layers such as input layer, pattern layer, summation layer, and output layer. The input layer feeds the input to the subsequent layer. The pattern layer determines the Euclidean distance and activation function. The number of neurons in this layer will be similar to the number of experiments used to train the network. The summation layer is made up of two subparts (that is the numerator and a denominator part of Eq. 2). The output layer consists of a single neuron that calculates the output by dividing the numerator and denominator parts of the summation layer. The typical structure of GRNN model developed in the current study is shown in Fig. 5.

The GRNN model predicts based on the Eq. 2.

$$\hat{Y}(X) = \left( \frac{\sum_{i=1}^n Y_i \exp\left(-\frac{D_i^2}{2\sigma^2}\right)}{\sum_{i=1}^n \exp\left(-\frac{D_i^2}{2\sigma^2}\right)} \right) \tag{2}$$

where  $\hat{Y}(X)$ = output predicted,  $X$ = input,  $Y_i$ = Output of the input sample  $I$ ,  $D_i^2$ = Euclidean distance from the  $X$  and  $X_i$ ,  $n$  = number of experiments,  $\sigma$  = spread parameter

The GRNN model output is calculated using the weighted average of the training dataset’s outputs. The weights are computed based on the Euclidean distance calculated

between the training data and test data. The Euclidean distances are calculated from training sample  $X_i$  using Eq. 3.

$$D_i^2 = (X - X_i)^T (X - X_i) \tag{3}$$

### 2.4 Adaptive neuro fuzzy inference system (ANFIS)

The general structure of the ANFIS model with three inputs (cutting speed, feed, and pecking depth) and single-output (thrust force) is presented in Fig. 6.

The ANFIS model consists of five layers; the initial layer is the fuzzification layer and consists of adaptable nodes. In order to obtain fuzzy datasets from input values, the fuzzification layer employs the Membership function (MF).

Many MF are available in ANFIS modelling, such as Trapezoidal and triangle MF, which are linear MF. Similarly, the Gaussian MF function processes non-linear input data. The combinational MF that combines different MF’s is also available. The type of MF affects the model prediction accuracy [47] and therefore, a suitable selection must be made.

Pi-membership function, abbreviated as Pi-MF, is selected for model development in the current study. Pi-MF is spline-based, pi-shaped, and combines an S-shaped and a Z-shaped MF and is shown in Eq. 4.

$$\mu_{Ai}(x) = PiMF(x; a, b, c, d) = \begin{cases} 0, & x \leq a \\ 2 \frac{(x-a)}{(b-a)^2}, & a \leq x \leq \frac{a+b}{2} \\ 1 - 2 \left( \frac{a-b}{b-a} \right)^2, & \frac{a+b}{2} \leq x \leq b \\ 1, & b \leq x \leq c \\ 1 - 2 \left( \frac{x-c}{d-c} \right)^2, & c \leq x \leq \frac{c+d}{2} \\ 2 \left( \frac{x-d}{d-c} \right)^2, & \frac{c+d}{2} \leq x \leq d \\ 0, & x \geq d \end{cases} \tag{4}$$

where  $a, b, c, d$  terms are called premise parameters, and the learning algorithm minimizes the training error by optimizing these terms.

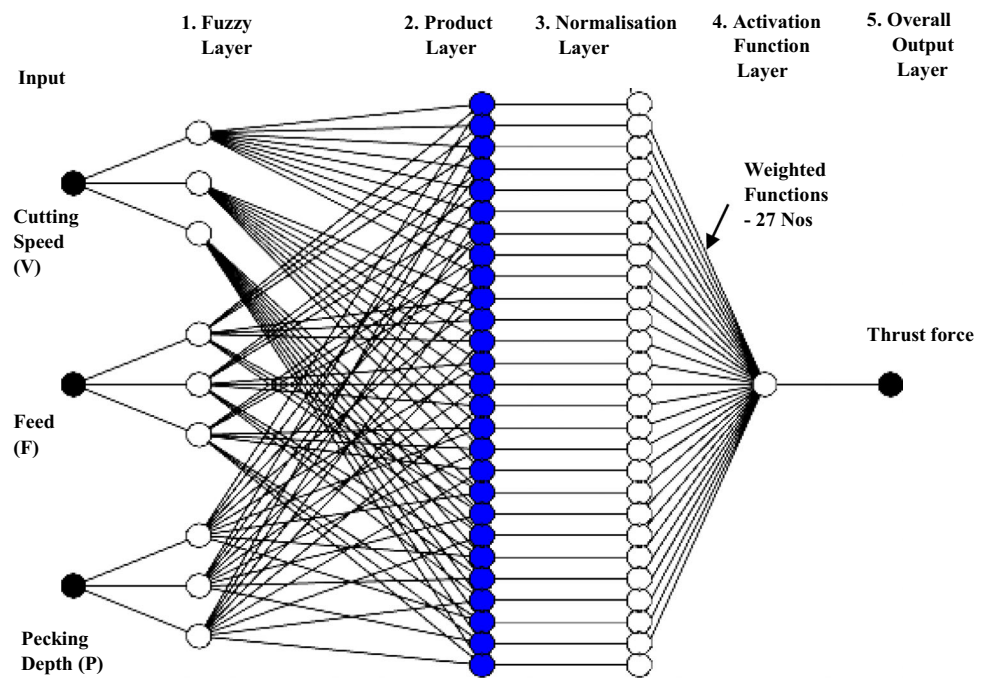
The second layer in the ANFIS structure is referred to as the rule layer and it consists of a fixed number of nodes. This layer is mainly responsible for generating firing strength ( $W_i$ ) for the rules using membership values computed in the previous layer. The values  $W_i$  are determined by multiplying the membership values as shown in the Eq. 5.

$$W_i = \mu_{Ai}(x) \cdot \mu_{Ai}(y) \cdot \mu_{Ai}(z) \quad i = 1, 2, 3 \dots 27 \tag{5}$$

where  $x, y, z$  are inputs  $\mu_{Ai}(x), \mu_{Ai}(y)$  and  $\mu_{Ai}(z)$  are membership functions and  $i$  is the number of rules generated (27 in the current study).



**Fig. 6** Block diagram of ANFIS architecture



The third layer is the normalization layer, which determines each rule’s normalized firing strengths. The normalized value for the  $i$ th rule is calculated as shown in Eq. 6.

$$\bar{W}_i = \frac{W_i}{\sum_i W_i} \quad i = 1, 2, 3 \dots 27 \tag{6}$$

The activation function layer is the fourth layer and each node of this layer determines the weighted values of rules by multiplying with a first-order polynomial as shown in Eq. 7.

$$\bar{W}_i \cdot f_i = W_i(p_i x + q_i y + r_i z) \tag{7}$$

where  $\bar{W}_i$  is normalisation layer output and  $f_i$  is activation function.

The nodes in this layer are adaptive and where constants in equation  $p_i, q_i$  and  $r_i$  (called as consequence parameters) have to be adjusted by the learning algorithm.

Finally, the fifth layer is referred to as the summation layer or overall output layer, and the final output of ANFIS is determined by summing the individual outputs of each rule of defuzzification layer as shown in Eq. 8.

$$\sum_{i=1}^{27} \bar{W}_i f_i = \frac{\sum_{i=1}^{27} W_i * f_i}{\sum_{i=1}^{27} W_i} \tag{8}$$

### 2.5 Multiple regression analysis

The Multiple Regression Analysis (MRA) combines statistical and mathematical techniques to analyse the effects of

many input process parameters on output responses. In MRA, the quadratic models of second order are found effective in modelling responses in MMD compared to bilinear models [35]. The second order quadratic models are also effective in predicting responses in others domains of mechanical engineering [32]. Therefore quadratic models of second-order are developed for the responses based on the Eq. 9 [48]

$$Y = \beta_0 + \sum_{i=1}^k \beta_i x_i + \sum_{i=1}^k \beta_{ii} x_i^2 + \sum_{j>1}^k \beta_{ij} x_i x_j \tag{9}$$

where  $y$  = output response,  $k$  = number of input process parameters,  $x_i, x_j$  input or process parameters,  $\beta_0$  is constant,  $\beta_i, \beta_{ii}, \beta_{ij}$  are coefficients of linear, square, and interaction terms.

### 3 Results and discussion

The experiments are carried out in three trials. The average value of measured responses is determined for each experiment and presented in Table 6.

The stereo microscope images of machined holes on the entry side of the workpiece under different experimental conditions are depicted in Fig. 7.

The data in Table 6 is used for training the GRNN and ANFIS models. The additional 10 data sets are generated by performing experiments at random points (not considered in the initial experimental design) to test and validate models and are presented in Table 7.

**Table 6** Experimental results –Training data

Exp. No	Cutting speed (m/min)	Feed ( $\mu\text{m}/\text{rev}$ )	Pecking depth (mm)	Experimental combination			Thrust force (N)	Burr height ( $\mu\text{m}$ )	Radial overcut ( $\mu\text{m}$ )
				V	F	P			
1	8.8	4	25	-1	-1	-1	8.94	30.30	11.250
2	8.8	4	50	-1	-1	0	9.41	30.57	11.900
3	8.8	4	75	-1	-1	+1	10.14	32.83	12.880
4	8.8	8	25	-1	0	-1	11.87	31.87	10.740
5	8.8	8	50	-1	0	0	13.26	32.40	12.440
6	8.8	8	75	-1	0	+1	13.20	34.47	12.500
7	8.8	12	25	-1	+1	-1	12.33	32.30	10.690
8	8.8	12	50	-1	+1	0	13.32	34.30	11.430
9	8.8	12	75	-1	+1	+1	14.58	36.47	12.865
10	13.8	4	25	0	-1	-1	9.15	30.73	13.100
11	13.8	4	50	0	-1	0	10.90	31.87	13.510
12	13.8	4	75	0	-1	+1	10.75	32.90	13.710
13	13.8	8	25	0	0	-1	10.39	30.13	13.880
14	13.8	8	50	0	0	0	11.17	32.37	14.450
15	13.8	8	75	0	0	+1	11.28	33.70	14.390
16	13.8	12	25	0	+1	-1	10.76	31.63	14.150
17	13.8	12	50	0	+1	0	12.77	33.53	15.030
18	13.8	12	75	0	+1	+1	12.81	35.67	15.170
19	18.8	4	25	+1	-1	-1	8.01	27.00	11.200
20	18.8	4	50	+1	-1	0	9.54	30.70	12.840
21	18.8	4	75	+1	-1	+1	9.80	31.23	13.580
22	18.8	8	25	+1	0	-1	8.89	29.20	13.780
23	18.8	8	50	+1	0	0	10.20	31.03	13.620
24	18.8	8	75	+1	0	+1	10.25	31.97	13.590
25	18.8	12	25	+1	+1	-1	10.29	30.97	15.590
26	18.8	12	50	+1	+1	0	11.81	33.03	15.810
27	18.8	12	75	+1	+1	+1	11.99	33.90	16.140

The prediction accuracy of the developed model is influenced by the spread parameter ( $\sigma$ ) value in the GRNN model and the type of MF in the ANFIS model. Therefore to minimize prediction errors, the datasets from experiments 1–5 in Table 7 are utilized to determine the optimal value of spread parameter in GRNN models and the best type of MF in ANFIS models. The developed models are validated using the datasets from experiments 6–10.

### 3.1 Predictive models

In the current study three modelling techniques are used to establish relationship between process parameters and responses. The performance of AI based GRNN, ANFIS models are compared with regression models developed by MRA.

#### 3.1.1 GRNN modelling

In the initial step, the spread parameter “ $\sigma$ ” is selected, and from Eq. 2 used for prediction in GRNN modelling, “ $\sigma$ ” is the only unknown parameter. The selection of “ $\sigma$ ” influences the prediction accuracy of GRNN models. The high value of “ $\sigma$ ” can result in under fitting, and the low-value results in overfitting. Therefore an optimal value has to be selected for the best performance of GRNN models.

No intuitive methods are available to choose the optimal spread parameter, and a trial and method must be applied [27, 30]. Since many computations are needed to calculate one set of variables, a *Matlab* spread parameter selection function is used for the implementation. The training data set is used as input (experimental data in Table 6), and a trial error method is applied to predict responses at different “ $\sigma$ ”

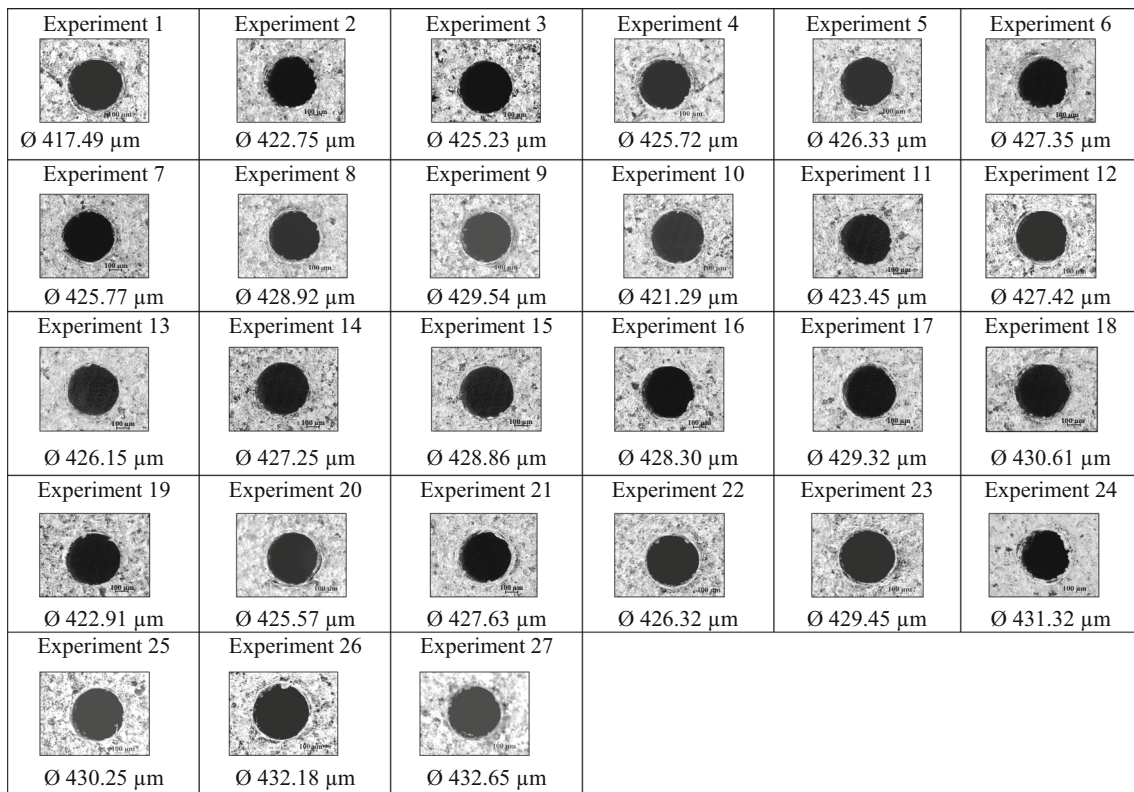


Fig. 7 Stereo microscope images of machined holes on the entry side

Table 7 Experimental results additional –testing and validation data

Exp. No	Cutting speed (m/min)	Feed (µm/rev)	Pecking depth (mm)	Experimental combination			Thrust force (N)	Burr height (µm)	Radial overcut (µm)
				V	F	P			
1	9.42	5	30	− 0.88	− 0.75	− 0.80	9.10	29.70	11.04
2	10.68	6.5	55	− 0.63	− 0.38	+ 0.20	12.26	30.95	12.22
3	11.30	9	65	− 0.50	+ 0.25	+ 0.60	12.90	35.75	14.03
4	12.56	9	70	− 0.25	+ 0.25	+ 0.80	11.92	33.15	14.21
5	17.58	10	45	+ 0.76	− 0.63	+ 0.40	9.43	31.20	15.02
6	16.96	5	35	+ 0.63	− 0.75	− 0.60	8.63	29.25	11.75
7	18.21	10	45	+ 0.88	+ 0.50	− 0.20	10.51	33.17	15.30
8	11.30	6	37.5	− 0.50	− 0.50	− 0.50	10.40	30.33	12.94
9	10.05	7.5	40	− 0.75	− 0.13	− 0.40	12.51	33.60	12.90
10	16.33	10	62.5	+ 0.50	+ 0.50	+ 0.50	12.11	33.70	14.31

and compared with the test data set (from experiments 1–5 in Table 7) for calculating mean absolute errors. The variation of mean absolute error with spread parameter for thrust force, burr height, and radial overcut models is depicted in Fig. 8.

The spread parameter value ( $\sigma$ ) at which minimum mean absolute error is observed represents the optimal value and is selected for developing the GRNN model. Therefore  $\sigma = 1.5$  is selected for developing the thrust force model, and

similarly,  $\sigma = 1.35$  and  $\sigma = 0.15$  are selected for developing burr height, and radial overcut models.

GRNN models are developed for thrust force, burr height and radial overcut using selected “ $\sigma$ ” values. The correlation between experimental values and their corresponding GRNN model predicted values for training data are depicted in Fig. 9.

From Fig. 9a, b, and c, it is observed that  $R^2$ -values are 1 for thrust force, burr height, and radial overcut models. Because the  $R^2$ -value of data is equal to a perfect fit value, the

**Fig. 8** Mean absolute error variation with spread parameter for test data

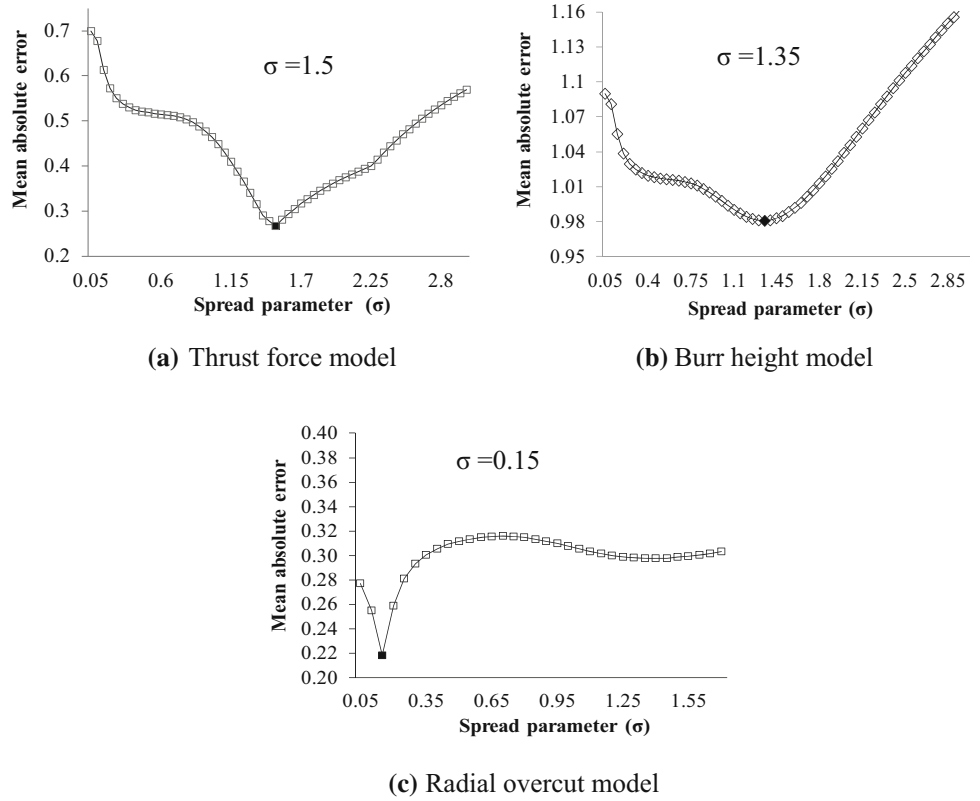
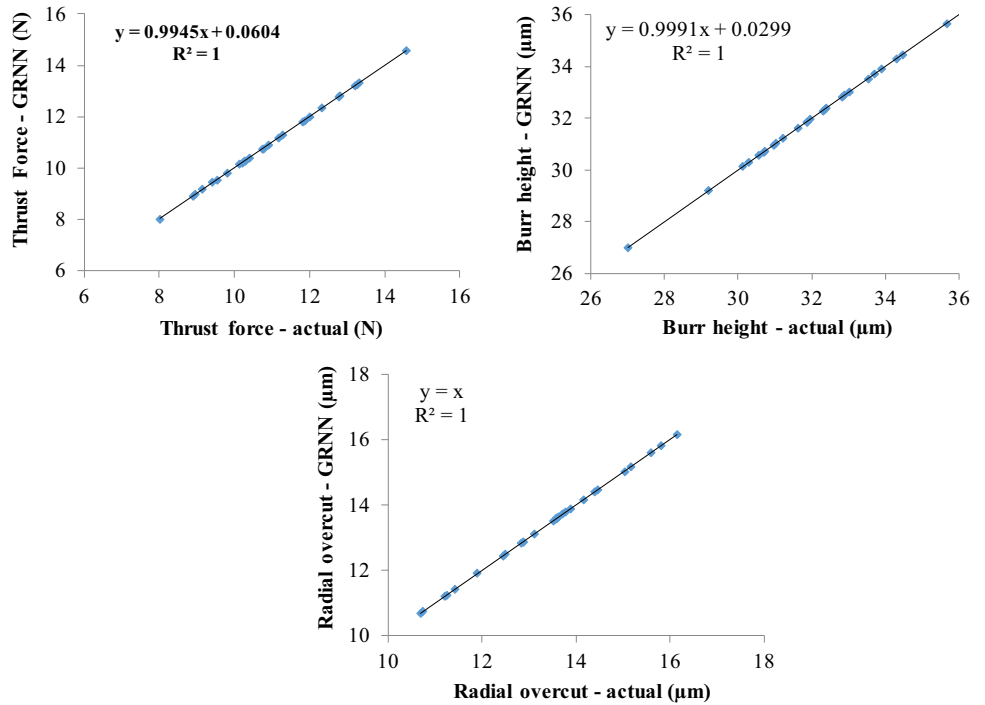


**Fig. 9** Correlation between experimental values and GRNN model predicted values for training data



trained network model's accuracy is high. Finally developed GRNN models are validated using validation data set (from experiments 6–10 in Table 7).

### 3.1.2 ANFIS modelling

ANFIS models are developed using *Matlab 2021a* based on experimental data in Table 6. In the initial step, the input data are normalized to get values ranging from 0 to 1 to compute ANFIS models.

In the next step, the Fuzzy Inference System (FIS) is selected, and in the ANFIS package, Sugeno and Mamdani FIS are commonly used to develop models. In Sugeno-FIS, the weighted average is used to de-fuzzify output, which reduces processing time and also improves computational accuracy [49]. Hence the Sugeno FIS is selected in the current study, and later developed models are trained by selecting parameters and optimization method.

For every input, three membership functions are selected, 27 rules are generated, and 550 epochs are used to train models [50]. Back-propagation and hybrid methods are currently available in the ANFIS package for training. The back-propagation method uses a gradient descent algorithm, which means that errors from each epoch are sent back to the network; this serves as feedback in self-correcting and self-learning [51]. Therefore, in current study back-propagation method is adopted for training.

In the final step, ANFIS models are developed by selecting a suitable Membership Function (MF). The current study evaluates different MF to select an MF that minimizes the prediction errors. After preliminary screening, trapezoidal-MF, Pi-MF, P-sigma-MF, and D-sigma-MF are considered for evaluation among the various MF provided in the ANFIS package. ANFIS models are developed for output responses such as thrust force, burr height, and radial overcut by providing the model's training data set as input (experimental data in Table 6). The type of MF is selected by comparing model predictions from various types of MF with actual experiment values in the test data set (from experiment 1–5 in Table 7). The prediction error is calculated using Eq. 10.

Prediction error (%)

$$= \frac{\text{Experimental value} - \text{predicted value}}{\text{Experimental value}} \quad (10)$$

The calculated absolute prediction error for thrust force, burr height and radial overcut models for different MF's is shown in Table 8. From Table 8, the minimum value of error is observed with Pi-MF.

The Fig. 10a shows the training process and selected parameters for thrust force model. The rule viewer in Fig. 10b depicts the prediction for experiment 1 in the test data set with the Pi-MF type in thrust force model.

The ANFIS models developed for thrust force, burr height and radial overcut by selecting Pi-MF is considered for prediction. The developed models are validated using validation data set (from experiment 6–10 in Table 7).

### 3.1.3 Multiple regression analysis (MRA) modelling

The quadratic second-order regression models are developed using *Minitab 17* statistical software. The actual values of the process parameters cutting speed (V), feed (F), and pecking depth (P) is transformed to coded units using Eqs. 11, 12 and 13.

$$X_1 = \left( \frac{V - V_0}{\Delta V} \right) \quad (11)$$

$$X_2 = \left( \frac{F - F_0}{\Delta F} \right) \quad (12)$$

$$X_3 = \left( \frac{P - P_0}{\Delta P} \right) \quad (13)$$

where  $X_1$ ,  $X_2$  and  $X_3$  are coded cutting speed V, feed F and pecking depth P,  $V_0$ ,  $F_0$  and  $P_0$  represent values of V, F and P at zero levels.  $\Delta V$ ,  $\Delta F$  and  $\Delta P$  are the interval of variation of V, F, and P respectively. The models developed for thrust force, burr height, and radial overcut in coded units is presented as Eqs. 14, 15, and 16.

$$\begin{aligned} \text{Thrust force} = & 11.592 - 0.904X_1 + 1.334X_2 \\ & + 0.787X_3 - 0.118X_1 * X_1 \\ & - 0.207X_2 * X_2 - 0.518X_3 * X_3 \\ & - 0.417X_1 * X_2 + 0.006X_1 * X_3 \\ & + 0.118X_2 * X_3 \end{aligned} \quad (14)$$

$$\begin{aligned} \text{Burr height} = & 32.380 - 0.916X_1 + 1.315X_2 \\ & + 1.612X_3 - 0.584X_1 * X_1 \\ & + 0.314X_2 * X_2 - 0.129X_3 * X_3 \\ & - 0.033X_1 * X_2 + 0.053X_1 * X_3 \\ & + 0.184X_2 * X_3 \end{aligned} \quad (15)$$

$$\begin{aligned} \text{Radial overcut} = & 14.184 + 1.081X_1 + 0.717X_2 \\ & + 0.580X_3 - 1.219X_1 * X_1 \\ & + 0.115X_2 * X_2 - 0.159X_3 * X_3 \\ & + 0.914X_1 * X_2 - 0.235X_1 * X_3 \\ & - 0.073X_2 * X_3 \end{aligned} \quad (16)$$



**Table 8** Prediction errors in ANFIS models with different membership functions

Sl No	Model	Membership function	Absolute prediction error (%)	Rank
1	Thrust force	Trapezoidal	5.53	2
		Pi	5.27	1
		P-sigma	11.51	3
		D-sigma	11.73	4
2	Burr height	Trapezoidal	5.85	2
		Pi	5.26	1
		P-sigma	8.49	3
		D-sigma	10.86	4
3	Radial overcut	Trapezoidal	6.86	2
		Pi	5.22	1
		P-sigma	8.15	3
		D-sigma	9.20	4

### 3.2 Comparison of developed models

The GRNN, ANFIS, and regression models developed for output responses thrust force, burr height, and radial overcut are used to predict at random points considered for validation (experiments 6–10 in Table 7). The prediction errors are determined by comparing GRNN, ANFIS and MRA model predicted values with actual experiment results using Eq. 10. The predicted responses from developed thrust force, burr height, and radial overcut models for testing and validation data are presented in Tables 9, 10, and 11 respectively.

The calculated MAPE for the GRNN, ANFIS and MRA models for testing and validation data is depicted in Fig. 11.

In thrust force model from Fig. 11a, the Maximum Absolute Prediction Error (MAPE) of 4.92%, 5.26%, and 11.69% with GRNN, ANFIS, and regression models respectively is observed. Similarly in burr height model in Fig. 11b, MAPE of 4.41%, 5.43%, and 9.27% are observed respectively with GRNN, ANFIS, and MRA models. Figure 11c depicts MAPE in radial overcut model of 4.68%, 5.22%, and 11.71% respectively with GRNN, ANFIS, and MRA models.

To the best of our knowledge, the literature is not available on the simultaneous development of GRNN and ANFIS and MRA prediction models to predict responses like thrust force, burr height, and radial overcut in the MMD process. Very few research works have been reported on applying AI tools like ANN and ANFIS in the MMD process, and the prediction results for responses of past studies are presented in Table 12.

In past studies on GRNN modelling in other machining processes, a mean prediction errors of 2.479% and 1.75% for kerf width and surface roughness in laser machining of stainless steels [26]. The mean prediction errors of 1.34% is observed for radial overcut in electro discharge machining of AISI D2 tool steel [21].

In past studies on ANFIS modelling in other machining processes, the mean prediction errors of 8.67% for material removal rate, 3.20% for tool wear rate, and 13.44% for diametric overcut in micro-electro discharge machining of silver [51]. The mean absolute prediction errors for material removal rate, surface roughness, and tool wear rate of 4.33%, 7.49%, and 6.37% in micro-electro discharge machining of stainless steel [52].

In the current study, mean prediction errors of 3.40% and 3.96% are observed in the prediction of thrust force in GRNN and ANFIS models for testing and validation data, respectively. The mean prediction errors of 2.67% and 3.19% are observed in the prediction of burr height in GRNN and ANFIS models for testing and validation data, respectively. Similarly, mean prediction errors of 2.53% and 2.84% are observed in the prediction of radial overcut in GRNN and ANFIS models for testing and validation data, respectively. The mean prediction errors observed in GRNN and ANFIS are in similar ranges of less than 5%, as observed in the literature.

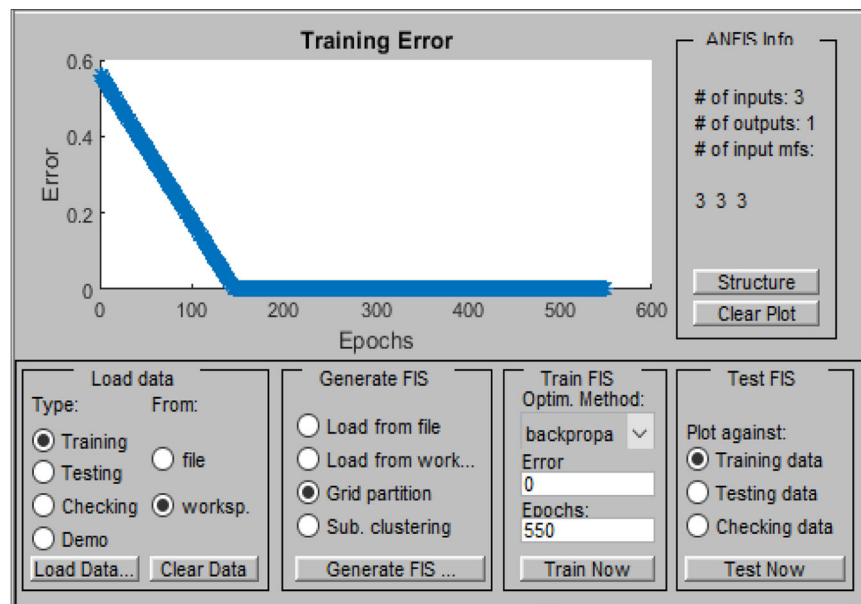
### 3.3 Influence of process parameters on responses

The ANOVA is performed at the desired confidence level of 95% to identify the significant process parameters and their contribution towards responses. The results of ANOVA are shown in Table 13.

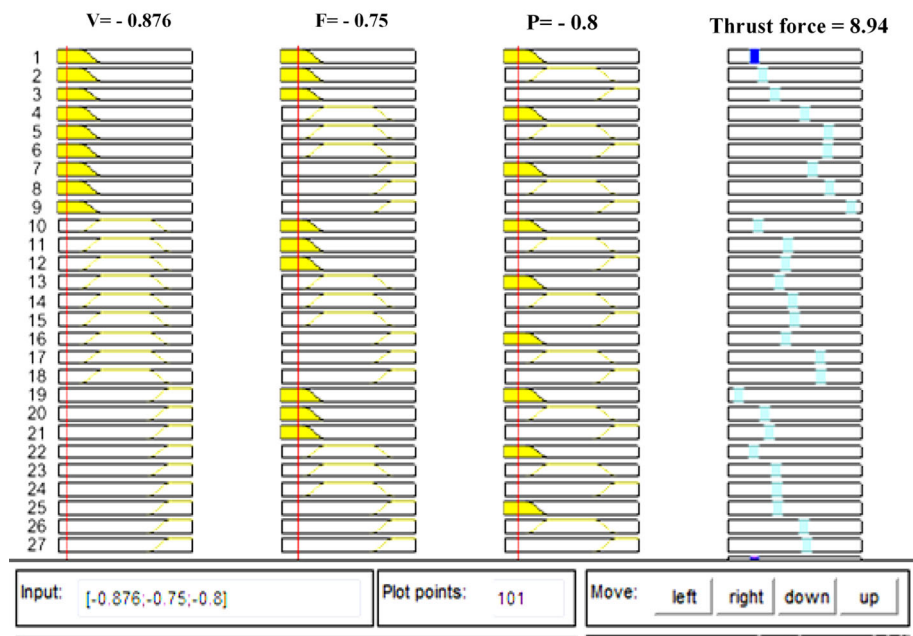
The bar charts are constructed using the average values of thrust force at each level of process parameters and depicted in Fig. 12.

From Fig. 12a illustrates a change in cutting speed from a lower to a higher level results in a decrease of 12.91% in thrust force. Higher cutting speeds cause thermal softening of the work material, which requires less force for chip removal, resulting in a lower thrust force. On the contrary,

**Fig. 10** ANFIS model of thrust force



**(a)** Variation of training with respect to epochs



**(b)** Rule viewer

increasing the feed from a lower to a higher level resulted in a 27.72% increase in thrust force. This trend can be attributed to increased chip load at the cutting edge due to increasing feed. On the other hand, the thrust force increased by 15.63% as the pecking depth increased from lower to higher levels. Chip clogging increases as pecking depth increases, resulting in more friction between drill flutes and hole wall, resulting in higher thrust force.

The ANOVA results in Table 13a feed; cutting speed, pecking depth, and the interaction term of cutting speed and feed are significant towards thrust force with a P-value of less than 0.05. Feed had a significant contribution of 46.52% towards thrust force followed by cutting speed, pecking depth, and interaction of cutting speed-feed at 21.34%, 16.19%, and 3.02%.

**Table 9** Predicted thrust force in testing and validation

Exp	Experimental combination			Actual thrust force (N)	Predicted thrust force (N)		
	V	F	P		GRNN	ANFIS	MRA
1	- 0.88	- 0.75	- 0.80	9.10	9.17	8.94	10.17
2	- 0.63	- 0.38	+ 0.20	12.26	12.23	12.27	11.69
3	- 0.50	+ 0.25	+ 0.60	12.90	12.35	12.23	12.64
4	- 0.25	+ 0.25	+ 0.80	11.92	11.44	11.28	12.43
5	+ 0.76	- 0.63	+ 0.40	9.43	9.71	9.67	10.45
6	+ 0.63	- 0.75	- 0.60	8.63	8.22	8.60	9.60
7	+ 0.88	+ 0.50	- 0.20	10.51	11.01	11.01	10.84
8	- 0.50	- 0.50	- 0.50	10.40	10.63	10.64	10.80
9	- 0.75	- 0.13	- 0.40	12.51	13.13	12.91	11.63
10	+ 0.50	+ 0.50	+ 0.50	12.11	11.51	11.52	11.81

**Table 10** Predicted burr height in testing and validation

Exp	Experimental combination			Actual burr height ( $\mu\text{m}$ )	Predicted burr height ( $\mu\text{m}$ )		
	V	F	P		GRNN	ANFIS	MRA
1	- 0.88	- 0.75	- 0.80	29.70	30.37	30.70	30.68
2	- 0.63	- 0.38	+ 0.20	30.95	32.09	32.20	32.56
3	- 0.50	+ 0.25	+ 0.60	35.75	34.17	33.70	33.48
4	- 0.25	+ 0.25	+ 0.80	33.15	33.80	33.90	34.15
5	+ 0.76	- 0.63	+ 0.40	31.20	30.77	31.50	31.86
6	+ 0.63	- 0.75	- 0.60	29.25	28.94	30.50	31.96
7	+ 0.88	+ 0.50	- 0.20	33.17	32.03	31.90	31.48
8	- 0.50	- 0.50	- 0.50	30.33	31.28	31.40	31.33
9	- 0.75	- 0.13	- 0.40	33.60	32.38	31.80	31.14
10	+ 0.50	+ 0.50	+ 0.50	33.70	33.11	33.10	31.44

**Table 11** Predicted radial overcut in testing and validation

Exp	Experimental combination			Actual radial overcut ( $\mu\text{m}$ )	Predicted radial overcut ( $\mu\text{m}$ )		
	V	F	P		GRNN	ANFIS	MRA
1	- 0.88	- 0.75	- 0.80	10.14	9.83	9.83	11.65
2	- 0.63	- 0.38	+ 0.20	12.22	12.44	12.57	13.14
3	- 0.50	+ 0.25	+ 0.60	14.03	13.96	13.45	13.76
4	- 0.25	+ 0.25	+ 0.80	14.46	14.39	14.39	14.36
5	+ 0.76	- 0.63	+ 0.40	15.24	14.72	14.71	13.62
6	+ 0.63	- 0.75	- 0.60	12.9	12.79	12.10	13.13
7	+ 0.88	+ 0.50	- 0.20	15.30	14.72	14.71	14.91
8	- 0.50	- 0.50	- 0.50	12.94	13.23	12.45	12.83
9	- 0.75	- 0.13	- 0.40	12.60	12.44	12.01	12.35
10	+ 0.50	+ 0.50	+ 0.50	14.31	14.79	14.77	15.21

**Fig. 11** Comparison between GRNN, ANFIS and MRA predicted values for testing and validation data

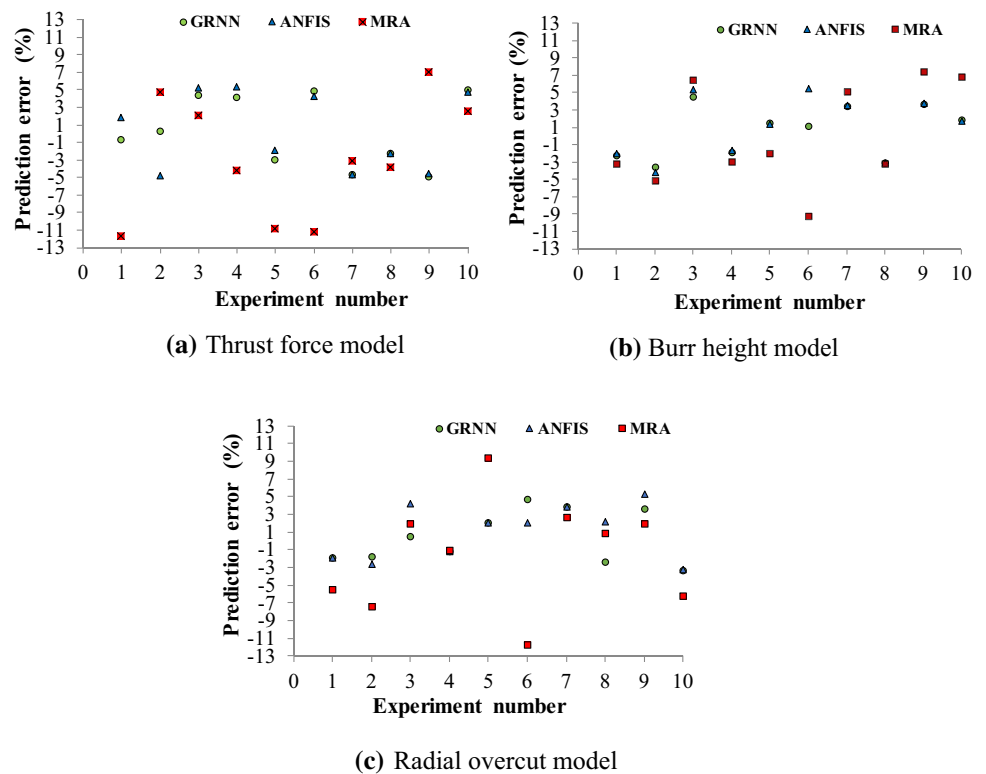


**Table 12** Prediction results of ANN and ANFIS models from past studies on MMD process

Sl No	Author	Workpiece material	Modelling/prediction tool	Process parameters	Responses	Mean prediction error (%)
1	Patra et al. (2015) [32]	Tool steel (AISI P20)	ANN	Cutting speed, feed rate, spindle speed and hole number	Chisel wear	3–6 (for different conditions)
2	Ranjan et al. (2020) [40]	Austenitic stainless steel SS316	ANFIS	Thrust force, torque and vibration signals	Roundness error	7.03
3	Huang et al. (2020) [39]	Aluminum 7075-T6 alloy	ANN	Nano diamond type, spindle speed, feed rate, distance of nozzle, MQL flow, air compression, pecking depth and angle of nozzle	Thrust force Torque	0.58 1.59

The bar chart in Fig. 13a indicates a 4.16% decrease in exit burr height as cutting speed increases from lower to higher levels. With higher cutting speeds, chip height decreases, leading to a reduction in burr heights [23]. On the contrary, an increase in burr height with a rise in feed and pecking depth is observed in Fig. 13b and c. This increasing trend in burr height can be attributed to the elevation of thrust forces during tool exit at higher feed and pecking depth. An increase in the feed from lower to higher levels results in an 8.51%

increase in exit burr height. Similarly, a rise in pecking depth from lower to higher levels causes a 10.58% rise in exit burr height.

From the ANOVA results in Table 13b, linear terms of pecking depth, cutting speed, and square term of cutting speed are significant towards exit burr height with P-value less than 0.05. The pecking depth significantly contributed with 45.12% towards exit burr height followed by feed, linear

**Table 13** ANOVA results

Source	DF	Adj SS	Adj MS	F-Value	P-Value	Contribution (%)	Rank	Remarks
<i>(a) Thrust force</i>								
V	1	14.706	14.706	36.820	< 0.001	21.34	2	Significant
F	1	32.053	32.053	80.250	< 0.001	46.52	1	Significant
P	1	11.155	11.155	27.930	< 0.001	16.19	3	Significant
V * V	1	0.084	0.084	0.210	0.652	0.12		
F*F	1	0.256	0.256	0.640	0.434	0.37		
P*P	1	1.612	1.612	4.040	0.061	2.34		
V*F	1	2.083	2.083	5.220	0.036	3.02	4	Significant
V* P	1	0.000	0.000	0.000	0.975	0.00		
F* P	1	0.166	0.166	0.410	0.528	0.24		
Error	17	6.791	0.399			9.85		
Total	26					100		R <sup>2</sup> = 90.15%
<i>(b) Burr height</i>								
V	1	15.088	15.088	34.400	< 0.001	14.56	3	Significant
F	1	31.126	31.126	70.960	< 0.001	30.04	2	Significant
P	1	46.754	46.754	106.590	< 0.001	45.12	1	Significant
V * V	1	2.050	2.050	4.670	0.045	1.98	4	Significant
F*F	1	0.591	0.591	1.350	0.262	0.57		
P*P	1	0.101	0.101	0.230	0.638	0.10		
V*F	1	0.013	0.013	0.030	0.864	0.01		
V* P	1	0.033	0.033	0.080	0.787	0.03		
F* P	1	0.407	0.407	0.930	0.349	0.39		
Error	17	7.457	0.439			7.20		
Total	26					100.00		R <sup>2</sup> = 92.80%
<i>(c) Radial overcut</i>								
V	1	21.028	21.028	101.21	< 0.001	35.19	1	Significant
F	1	9.252	9.252	44.53	< 0.001	15.48	3	Significant
P	1	6.061	6.061	29.17	< 0.001	10.14	5	Significant
V * V	1	8.910	8.910	42.89	< 0.001	14.91	4	Significant
F*F	1	0.079	0.079	0.38	0.546	0.13		
P*P	1	0.151	0.151	0.73	0.406	0.25		
V*F	1	10.019	10.019	48.23	< 0.001	16.77	2	Significant
V* P	1	0.665	0.665	3.20	0.091	1.11		
F* P	1	0.064	0.064	0.31	0.587	0.11		
Error	17	3.532	0.208			5.91		
Total	26					100.00		R <sup>2</sup> = 94.09%

cutting speed, and square term of cutting speed at 30.04%, 14.56%, and 1.98%, respectively.

From Fig. 14a, a more significant radial overcut is observed with higher cutting speed due to increased drill wandering motion during entry. An increase of 19.21% in radial overcut is observed due to a rise in cutting speed from lower to higher levels.

A similar trend is also observed with a change in feed and pecking depth in Fig. 14b and c. With the increase in feed,

chip size also becomes larger [5], and due to this, chip evacuation becomes difficult, resulting increase of lateral forces causing more overcut (similar results were observed in MMD of nickel-based super-alloy by Zhou et al. [53]). An increase of 11.32% is observed in radial overcut by a rise in the feed from lower to higher levels.

With higher pecking depth, chip length also increases, resulting in more wandering motion due to chip entangling with the flute, and therefore more radial overcut is observed on the hole entry side. The increase of 9.13% in radial overcut



**Fig. 12** Mean variation of thrust force with cutting speed, feed and pecking depth

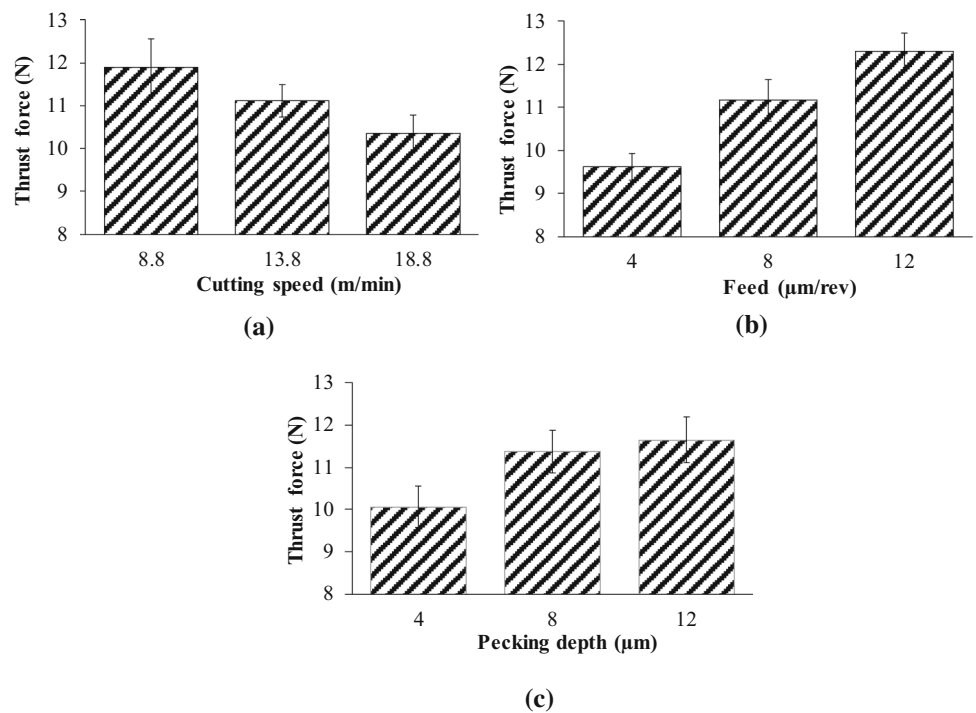
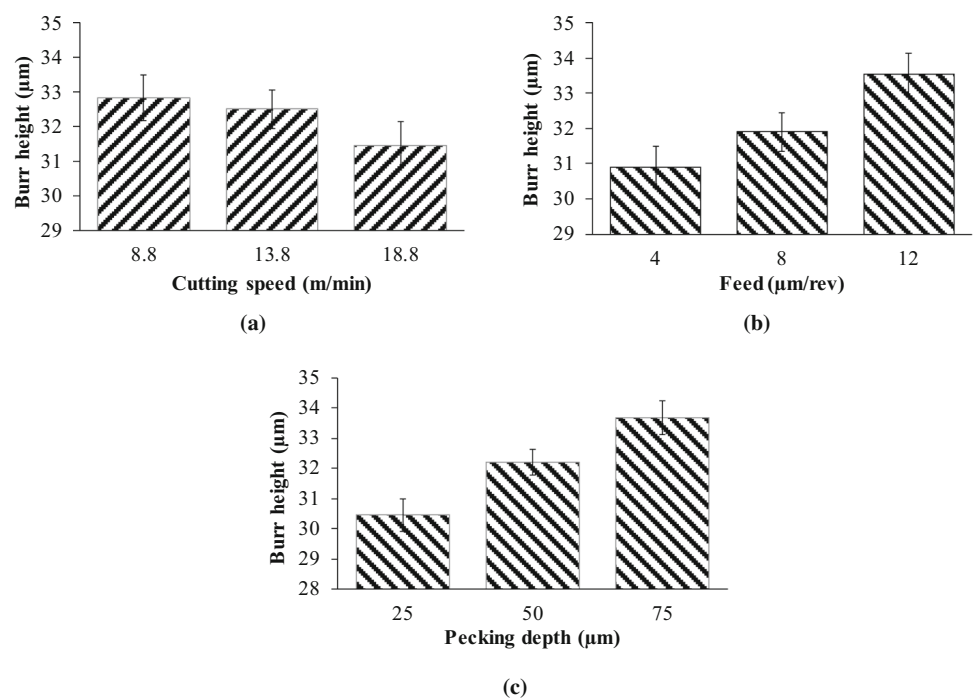


**Fig. 13** Mean variation of burr height with cutting speed, feed and pecking depth



is observed due to a rise in pecking depth from lower to higher levels.

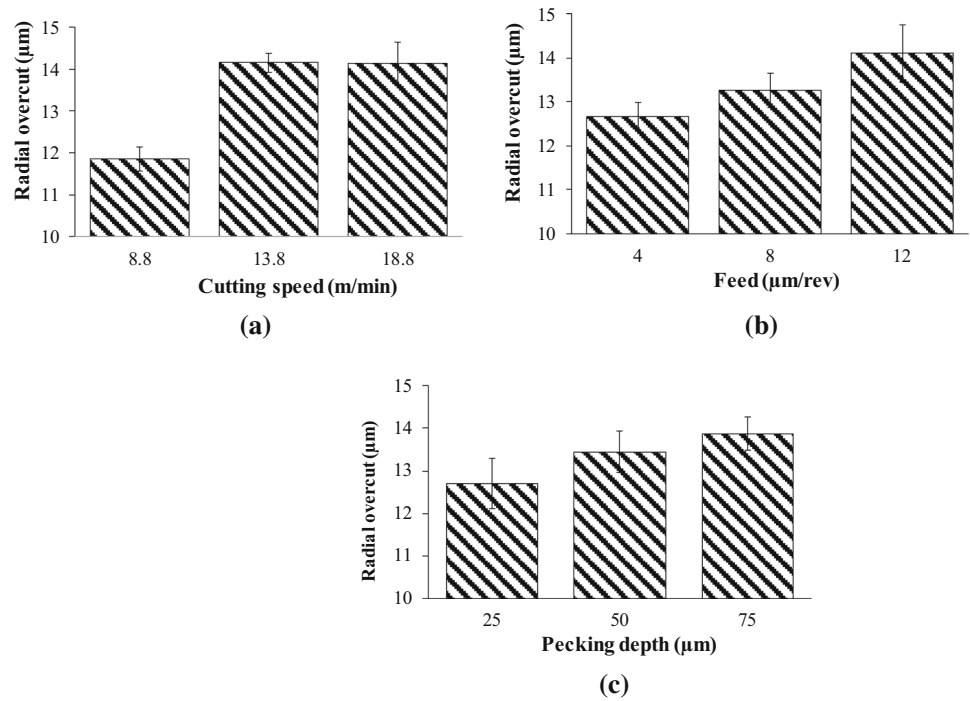
From the ANOVA results in Table 13c, the linear terms of cutting speed, feed, pecking depth, square term of cutting speed, and the interaction term of cutting speed and feed are significant towards radial overcut with P-value less than 0.05. Linear cutting speed has significantly contributed with 35.19% followed by interaction term of cutting speed and

feed, linear term of feed, square term of cutting speed, and linear term of pecking depth at 16.77%, 15.48%, 14.91%, and 10.14%, respectively.

### 3.4 Multi-response optimization

From the previous section, it is observed that a unique optimal solution to optimize all responses is not available; therefore

**Fig. 14** Mean variation of radial overcut with cutting speed, feed, and pecking depth



multi-response optimization is carried out to obtain a single optimal solution. The Desirability Function Analysis (DFA) method is implemented for multi-response optimization. In DFA, desirability values ranging from 0 to 1 are calculated using desirability functions. In the current study, responses like thrust force, exit burr height, and radial overcut should be minimized; hence smaller the better desirability function is used. A composite desirability value is determined by assigning equal weights to the desirability values of individual responses. The process parameter setting where the maximum composite desirability value is observed represents an optimal condition.

The results of DFA are presented in Fig. 15. The optimal process parameter setting is obtained at cutting speed of 18.8 m/min, feed of 4 µm/rev, and pecking depth of 25 µm.

### 3.5 Comparison of Ti–Al–N coated and uncoated tools

In this section, 20 holes are machined at fixed condition of process parameters, at optimal cutting speed 18.8 m/min, feed 4 µm/rev, and pecking depth 25 µm obtained previously from DFA. An uncoated carbide micro-drill of same length and similar geometry is used to machine 20 holes at optimal conditions. The performance of both the drills are analysed in terms of thrust force, exit burr height and radial overcut. This provides an insight on the influence of tool wear progress towards the responses while machining at a fixed condition (optimal process parameter settings).

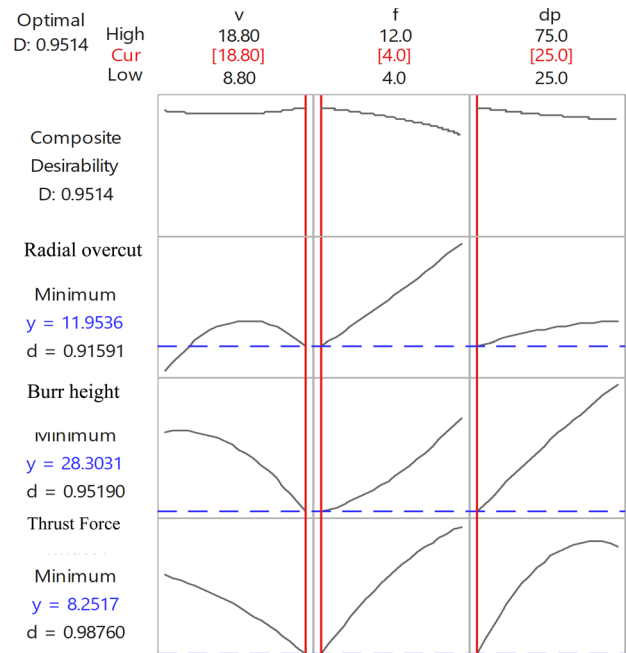


**Fig. 15** Multi response optimization plot

The Fig. 16 shows an increase in thrust force with the number of holes machined for both the micro-drills. A similar trend can also be observed in exit burr height, and radial overcut.

The coefficient of variation is calculated for comparing the performances of micro-drills based on the variability in measured response values of twenty holes machined. The

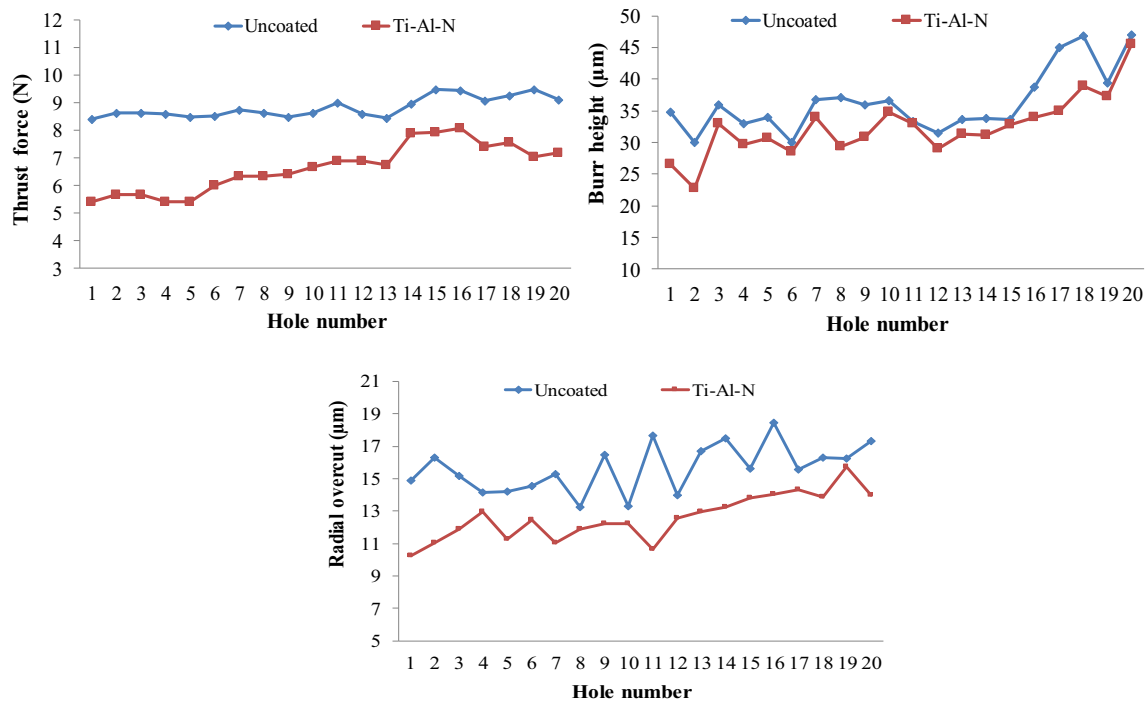


Fig. 16 Variation of responses with number of holes machined

Coefficient of Variation (*CV*) is a statistical measure is used; *CV* represents variability in sample of measured values of individual responses. *CV* is calculated using Eq. 17 in percentage [54].

$$CV(\%) = \frac{\text{standard deviation of sample}}{\text{Mean of sample}} \times 100 \quad (17)$$

The *CV* of 6.59% and 5.43% in thrust force, 13.67% and 11.65% in burr height, 10.04% and 9.72% in radial overcut with uncoated and Ti–Al–N micro-drill are observed, respectively. The Ti–Al–N coated micro-drill displayed a better performance as the lower coefficient of variation is observed compared to the uncoated tool for all responses.

### 3.5.1 Tool wear

The tool wear after machining twenty holes using both uncoated and the Ti–Al–N coated micro-drills is also compared and image of the tooltip before and after machining is shown in Fig. 17.

From Fig. 17, the dominant wear mechanism observed is adhesion and abrasion. The adhesion of work material due to affinity with the tool is observed more with the uncoated tool than Ti–Al–N coated tool. The low thermal conductivity of Titanium alloy (Cp–Ti grade 2) and machining under dry conditions also contributes to high chip tool interface temperature causing adhesion wear [8].

The wear on the flank surface is observed in both the tools due to material adhesion and abrasion during machining. The flank wear is measured after machining twenty holes using a stereomicroscope, the maximum flank wear value of 28.09 µm for uncoated micro-drill and 19.30 µm for Ti–Al–N coated micro-drill are observed. The magnitude of flank wear is found more in the uncoated micro-drill, and clear evidence of chipping of cutting edges is observed.

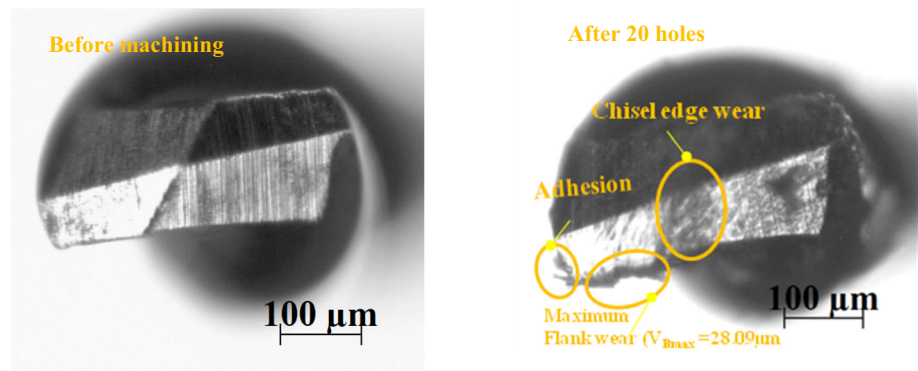
The Fig. 17 also reveals the chisel edge wear in both the micro-drills after machining, caused mainly due to abrasion and blunting of chisel edge is also noticed.

### 3.5.2 Chip morphology

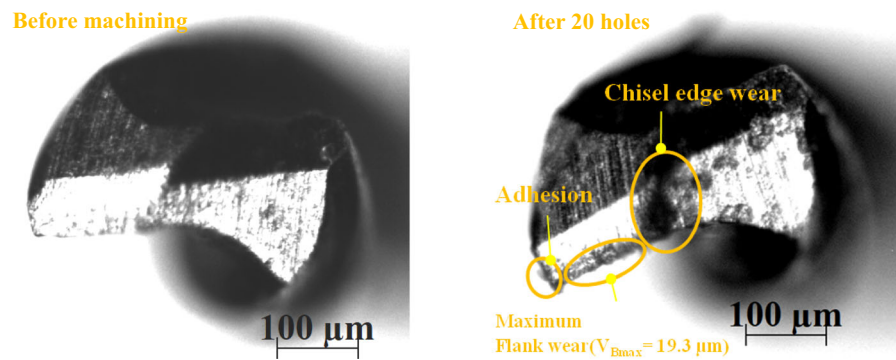
The current study is concluded with an analysis of chip morphology. The morphology of the formed chips determines the ease with which the drilling process is carried out. In orthogonal cutting processes such as turning and milling formation of chips ends as they leave the cutting edges, whereas in drilling chips flows along the flutes even after they are formed. Due to the complex shape of the drill with spiral flutes, the chips are not uniformly generated. The chips formed during holes machined at optimal settings to study tool wear are collected. The SEM images of typical continuous spiral chips generated are presented in Fig. 18.

In the current study, continuous spiral chips are formed with uncoated micro-drill whereas squeezed continuous spiral chips are formed with Ti–Al–N coated micro-drill. As

**Fig. 17** Stereo microscope images of tool tip



**(a)** Uncoated micro-drill



**(b)** Ti-Al-N coated micro-drill

shown in Fig. 18a, squeezed spiral chips are observed with the uncoated micro-drill can be attributed to high temperature at the chip tool interface during machining. Therefore chips formed get welded to the cutting edge, thus obstructing the flow resulting in squeezed spiral chips entangling between the flutes and work-piece surface [55]. The pitch between the spirals is also lesser due to the squeezing; hence the chips do not break easily. These reasons eventually cause an increase in thrust forces due to difficulties in chip evacuation and also elevate wandering motion causing more radial overcut.

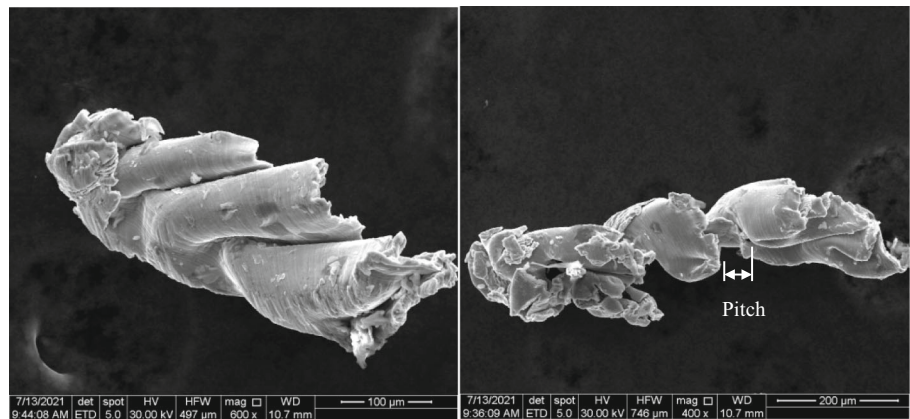
On the contrary, with the Ti–Al–N coated micro-drill, chips formed due to deformation flow easily in a continuous spiral form, as shown in the Fig. 18b, which is easier to evacuate. Therefore, the coating on the tool is found effective in reducing the temperature at the chip tool interface. Moreover, the chips have a larger pitch between spirals and breaks, easily indicating ease of machining hence generates lesser thrust forces than uncoated tool.

## 4 Conclusion

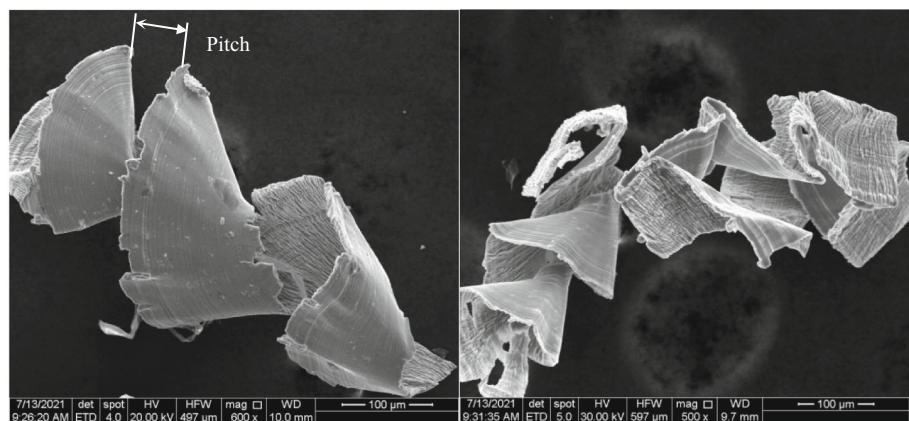
The mechanical micro-drilling process is carried out in the current study under dry conditions to machine micro-holes on Titanium: Cp-Ti grade-2 using  $\varnothing$  0.4 mm Ti–Al–N coated micro-drills. The current study develops predictive models for thrust force, burr height, and radial overcut using Generalised Regression Neural Network (GRNN), Adaptive Neuro-Fuzzy Inference System (ANFIS), and Multiple Regression Analysis (MRA) techniques. The experimental data generated based on the full-factorial design by varying cutting speed, feed, and pecking depth is used to train models. The model's performance is evaluated based on data generated by additional experiments for testing and validation. The major findings of the study are:

- Both GRNN and ANFIS models are more effective in predicting all responses than MRA models. Among them, GRNN models showed better performance with Maximum Absolute Prediction Error (MAPE) of 4.92%, 4.41%, and 4.68% in predicting thrust force, burr height, and radial overcut compared to the ANFIS model with MAPE of 5.27%, 5.17%, and 5.22%, Whereas MRA models

**Fig. 18** Chips formed at  $V = 18.8$  m/min,  $F = 4$   $\mu\text{m}/\text{rev}$  and  $P = 25$   $\mu\text{m}$



(a) Chips formed with uncoated micro-drill



(b) Chips formed with Ti-Al-N coated micro-drill

predicted with MAPE of 11.72%, 9.27%, and 11.71% respectively.

- The effects of process parameters on output responses is analyzed using ANOVA. The results suggest that feed and pecking depth played a significant role in increasing thrust force and burr height, respectively while cutting speed increases the radial overcut considerably.
- The multi-response optimization is carried out using DFA and optimal process parameter settings to simultaneously minimize responses is obtained at cutting speed of 18.8 m/min, feed of 4  $\mu\text{m}/\text{rev}$ , and pecking depth of 25  $\mu\text{m}$ . The average thrust force of 6.65 N, average burr height of 32.40  $\mu\text{m}$  and radial overcut of 12.60  $\mu\text{m}$ .
- At optimal parameters, the performance of the Ti–Al–N coated, uncoated micro-drills is evaluated by carrying out additional experiments. Compared to an uncoated micro-drill, the Ti–Al–N coated micro-drill showed a reduction in average thrust force from 8.83 to 6.65 N (24.68%), average burr height from 36.33 to 32.40  $\mu\text{m}$  (10.81%), and average radial overcut from 15.64 to 12.61  $\mu\text{m}$  (19.36%).

- In the tool wear analysis and chip formation, Ti–Al–N coated micro-drill effectively reduced flank wear from 28.09 to 19.30  $\mu\text{m}$  (31.29%) compared to the uncoated micro-drill. Continuous spiral chips are observed with Ti–Al–N coated micro-drill, indicating ease of machining compared to squeeze continuous spiral chips formed with uncoated micro-drill.

The current research can be extended to model other quality attributes like cylindricity and surface roughness under minimum quantity lubrication and other near-dry machining conditions.

## Declarations

**Conflict of interest** Authors declare that they have no known competing financial interests or personal relationships that could have appeared to influence the work reported in this paper.



## References

- Ramsden, J.J., Allen, D.M., Stephenson, D.J., Alcock, J.R., Peggs, G.N., Fuller, G., Goch, G.: The design and manufacture of biomedical surfaces. *CIRP Ann. Manuf. Technol.* **56**(2), 687–711 (2007)
- Anasane, S.S., Bhattacharyya, B.: Parametric analysis of fabrication of through micro holes on titanium by maskless electrochemical micromachining. *Int. J. Adv. Manuf. Technol.* **105**(11), 4585–4598 (2019)
- Sharma, N., Ahuja, N., Goyal, R., Rohilla, V.: Parametric optimization of EDD using RSM-Grey-TLBO-based MCDM approach for commercially pure titanium. *Grey Syst. Theory Appl.* **10**(2), 231–245 (2020)
- Rahamathullah, I., Shunmugam, S.: Thrust and torque analyses for different strategies adapted in microdrilling of glass-fibre-reinforced plastic. *Proc. Inst. Mech. Eng. Part B J. Eng. Manuf.* **225**(4), 505–519 (2011)
- Ming, W., Dang, J., An, Q., Chen, M.: Chip formation and hole quality in dry drilling additive manufactured Ti6Al4V. *Mater. Manuf. Process.* **35**(1), 43–51 (2020)
- Niinomi, M.: Recent titanium R&D for biomedical applications in Japan. *Jom* **51**(6), 32–34 (1999)
- Jawahir, I.S., Puleo, D.A., Schoop, J.: Cryogenic machining of biomedical implant materials for improved functional performance, life and sustainability. *Procedia CIRP* **46**, 7–14 (2016)
- Khan, A., Maity, K.: Influence of cutting speed and cooling method on the machinability of commercially pure titanium (CP-Ti) grade II. *J. Manuf. Process.* **31**, 650–661 (2018)
- Yongchen, P., Qingchang, T., Zhaojun, Y.: A study of dynamic stresses in micro-drills under high-speed machining. *Int. J. Mach. Tools Manuf.* **46**(14), 1892–1900 (2006)
- Bagci, E., Ozcelik, B.: Investigation of the effect of drilling conditions on the twist drill temperature during step-by-step and continuous dry drilling. *Mater. Des.* **27**(6), 446–454 (2006)
- Rahamathullah, I., Shunmugam, M.S.: Analyses of forces and hole quality in micro-drilling of carbon fabric laminate composites. *J. Compos. Mater.* **47**(9), 1129–1140 (2013)
- Kim, H.N.: Micro deep hole drilling operation technique. *J. Korean Soc. Mach. Tool Eng.* **8**(1), 15–20 (1999)
- Han, J.U., Won, J.S., Jung, Y.G.: An experimental study on micro drilling using step feed. *J. Korean Soc. Precis. Eng.* **13**(12), 46–53 (1996)
- Kim, D.W., Lee, Y.S., Park, M.S., Chu, C.N.: Tool life improvement by peck drilling and thrust force monitoring during deep-micro-hole drilling of steel. *Int. J. Mach. Tools Manuf.* **49**(3–4), 246–255 (2009)
- Imran, M., Mativenga, P.T., Kannan, S., Novovic, D.: An experimental investigation of deep-hole microdrilling capability for a nickel-based superalloy. *Proc. Inst. Mech. Eng. Part B J. Eng. Manuf.* **222**(12), 1589–1596 (2008)
- Kang, M.C., Je, S.K., Kim, K.H., Shin, B.S., Kwon, D.H., Kim, J.S.: Cutting performance of CrN-based coatings tool deposited by hybrid coating method for micro drilling applications. *Surf. Coatings Technol.* **202**(22–23), 5629–5632 (2008)
- Kao, W.H.: High-speed drilling performance of coated micro-drills with Zr-C-H:Nx% coatings. *Wear* **267**(5–8), 1068–1074 (2009)
- Imran, M., Mativenga, P.T., Gholinia, A., Withers, P.J.: Comparison of tool wear mechanisms and surface integrity for dry and wet micro-drilling of nickel-base superalloys. *Int. J. Mach. Tools Manuf.* **76**, 49–60 (2014)
- Swain, N., Kumar, P., Srinivas, G., Ravishankar, S., Barshilia, H.C.: Mechanical micro-drilling of nimonic 80A superalloy using uncoated and TiAlN-coated micro-drills. *Mater. Manuf. Process.* **32**(13), 1537–1546 (2017)
- Giorleo, L., Ceretti, E., Giardini, C.: ALD coated tools in micro drilling of Ti sheet. *CIRP Ann. Manuf. Technol.* **60**(1), 595–598 (2011)
- Guu, Y.H., Deng, C.S., Hou, M.T.K., Hsu, C.H., Tseng, K.S.: Optimization of machining parameters for stress concentration in microdrilling of titanium alloy. *Mater. Manuf. Process.* **27**(2), 207–213 (2012)
- Prasanna, J., Karunamoorthy, L., Venkat Raman, M., Prashanth, S., Raj Chordia, D.: Optimization of process parameters of small hole dry drilling in Ti-6Al-4V using Taguchi and grey relational analysis. *Meas. J. Int. Meas. Confed.* **48**(1), 346–354 (2014)
- Perçin, M., Aslantas, K., Uçun, I., Kaynak, Y., Çicek, A.: Microdrilling of Ti-6Al-4V alloy: the effects of cooling/lubricating. *Precis. Eng.* **45**, 450–462 (2016)
- Nam, J., Lee, S.W.: Machinability of titanium alloy (Ti-6Al-4V) in environmentally-friendly micro-drilling process with nanofluid minimum quantity lubrication using nanodiamond particles. *Int. J. Precis. Eng. Manuf. Green Technol.* **5**(1), 29–35 (2018)
- Mittal, R.K., Yadav, S., Singh, R.K.: Mechanistic force and burr modeling in high-speed microdrilling of Ti6Al4V. *Procedia CIRP* **58**, 329–334 (2017)
- Ding, H., Wang, Z., Guo, Y.: Infrared physics & technology multi-objective optimization of fiber laser cutting based on generalized regression neural network and non-dominated sorting genetic algorithm. *Infrared Phys. Technol.* **108**, 609–628 (2020)
- Panda, B.N., Bahubalendruni, M.V.A.R., Biswal, B.B.: A general regression neural network approach for the evaluation of compressive strength of FDM prototypes. *Neural Comput. Appl.* **26**(5), 1129–1136 (2015)
- Panda, B.N., Bahubalendruni, M.R., Biswal, B.B.: Optimization of resistance spot welding parameters using differential evolution algorithm and GRNN. In: *Proceedings of the 2014 IEEE 8th International Conference on Intelligent Systems and Control (ISCO)*, pp. 50–55 (2014)
- Kumar, S.: Environmental effects comparison of linear regression and artificial neural network technique for prediction of a soybean biodiesel yield. *Energy Sources Part A Recover. Util. Environ. Eff.* **42**(12), 1–11 (2019)
- Pradhan, M.K., Das, R.: Application of a general regression neural network for predicting radial overcut in electrical discharge machining of AISI D2 tool steel. *Int. J. Mach. Mach. Mater.* **17**(3–4), 355–369 (2015)
- Majumder, H., Maity, K.P.: Predictive analysis on responses in WEDM of titanium grade 6 using general regression neural network (GRNN) and multiple regression analysis (MRA). *SILICON* **10**(4), 1763–1776 (2018)
- Kumar, S., Jain, S., Kumar, H.: Application of adaptive neuro-fuzzy inference system and response surface methodology in biodiesel synthesis from jatropha e algae oil and its performance and emission analysis on diesel engine coupled with generator. *Energy* **226**, 120428 (2021)
- Kumar, S.: Production and optimization from Karanja oil by adaptive neuro-fuzzy inference system and response surface methodology with modified domestic microwave. *Fuel* **296**, 120684 (2021)
- Kumar, S.: Estimation capabilities of biodiesel production from algae oil blend using adaptive neuro-fuzzy inference system (ANFIS). *Energy Sources Part A Recover. Util. Environ. Eff.* **42**(7), 909–917 (2020)
- Patra, K., Anand, R.S., Steiner, M., Biermann, D.: Experimental analysis of cutting forces in microdrilling of austenitic stainless steel (X5CrNi18-10). *Mater. Manuf. Process.* **30**(2), 248–255 (2015)
- Ahn, Y., Lee, S.H.: Classification and prediction of burr formation in micro drilling of ductile metals. *Int. J. Prod. Res.* **55**(17), 4833–4846 (2017)

37. Patra, K., Jha, A.K., Szalay, T., Ranjan, J., Monostori, L.: Artificial neural network based tool condition monitoring in micro mechanical peck drilling using thrust force signals. *Precis. Eng.* **48**, 279–291 (2017)
38. Anand, R.S., Patra, K.: Cutting force and hole quality analysis in micro-drilling of CFRP. *Mater. Manuf. Process.* **33**(12), 1369–1377 (2018)
39. Huang, W.T., Chen, J.T.: Application of intelligent modeling methods to enhance the effectiveness of nanofluid/micro lubrication in microdeep drilling holes machining. *J. Adv. Mech. Des. Syst. Manuf.* **14**(7), 1–26 (2020)
40. Ranjan, J., Patra, K., Szalay, T., Mia, M., Gupta, M.K.: Artificial intelligence-based hole quality prediction. *Sensors* **20**, 1–14 (2020)
41. Ravisubramanian, S., Shunmugam, M.S.: Investigations into peck drilling process for large aspect ratio microholes in aluminum 6061-T6. *Mater. Manuf. Process.* **33**(9), 935–942 (2018)
42. Eltaggaz, A., Deiab, I.: Comparison of between direct and peck drilling for large aspect ratio in Ti-6Al-4V alloy. *Int. J. Adv. Manuf. Technol.* **102**(9–12), 2797–2805 (2019)
43. Stein, J.M., Dornfeld, D.A.: Burr formation in drilling miniature holes. *CIRP Ann. Manuf. Technol.* **46**(1), 63–66 (1997)
44. Pramanik, A., Basak, A.K., Uddin, M.S., Shankar, S., Debnath, S., Islam, M.N.: Burr formation during drilling of mild steel at different machining conditions. *Mater. Manuf. Process.* **34**(7), 726–735 (2019)
45. Jafferson, J.M., Hariharan, P.: Investigation of the quality of microholes machined by  $\mu$ EDM using image processing. *Mater. Manuf. Process.* **28**(12), 1356–1360 (2013)
46. Hiremath, S.S., Raju, L.: Investigation on machining copper plates with NiP coated tools using tailor-made micro-electro discharge machine. *Adv. Mater. Process. Technol.* **3**(4), 522–538 (2017)
47. Swain, A., Das, M.K.: Artificial intelligence approach for the prediction of heat transfer coefficient in boiling over tube bundles. *Proc. Inst. Mech. Eng. Part C J. Mech. Eng. Sci.* **228**(10), 1680–1688 (2014)
48. Farid, A.A., Sharif, S., Ashrafi, S.A., Idris, M.H.: Statistical analysis, modeling, and optimization of thrust force and surface roughness in high-speed drilling of Al-Si alloy. *Proc. Inst. Mech. Eng. Part B J. Eng. Manuf.* **227**(6), 808–820 (2013)
49. Hamam, A., Georganas, N.D.: A comparison of mamdani and sugeno fuzzy inference systems for evaluating the quality of experience of haptic-audio-visual applications. In: *HAVE 2008 IEEE international workshop haptic audio visual environments and games proceedings*, pp. 87–92. (2008)
50. Palanisamy, D., Senthil, P.: Development of ANFIS model and machinability study on dry turning of cryo-treated PH stainless steel with various inserts. *Mater. Manuf. Process.* **32**(6), 654–669 (2017)
51. Bhiradi, I., Raju, L., Hiremath, S.S.: Adaptive neuro-fuzzy inference system (ANFIS): modelling, analysis, and optimisation of process parameters in the micro-EDM process. *Adv. Mater. Process. Technol.* **6**(1), 133–145 (2020)
52. Suganthi, X.H., Natarajan, U., Sathiyamurthy, S., Chidambaram, K.: Prediction of quality responses in micro-EDM process using an adaptive neuro-fuzzy inference system (ANFIS) model. *Int. J. Adv. Manuf. Technol.* **68**(1–4), 339–347 (2013)
53. Zhou, Y., Li, H., Ma, L., Chen, J., Tan, Y., Yin, G.: Study on hole quality and surface quality of micro-drilling nickel-based single-crystal superalloy. *J. Brazilian Soc. Mech. Sci. Eng.* **42**(6), 1–13 (2020)
54. Bindu, K.H., Raghava, M., Dey, N., Rao, C.R.: *Coefficient of variation and machine learning applications*. CRC Press, Boca Raton (2019)
55. Gajrani, K.K., Divse, V., Joshi, S.S.: Burr reduction in drilling titanium using drills with peripheral slits. *Trans. Indian Inst. Met.* **74**(5), 1155–1172 (2021)

**Publisher's Note** Springer Nature remains neutral with regard to jurisdictional claims in published maps and institutional affiliations.

Springer Nature or its licensor holds exclusive rights to this article under a publishing agreement with the author(s) or other rightsholder(s); author self-archiving of the accepted manuscript version of this article is solely governed by the terms of such publishing agreement and applicable law.